LANGEVIN EQUATION FOR DIFFUSION OF MOLECULES ADSORBED ON SURFACES

by
Patrick Shea

Submitted in partial fulfillment of the
requirements for the degree of
Master of Science

at

Dalhousie University
Halifax, Nova Scotia
July 2010

DALHOUSIE UNIVERSITY

DEPARTMENT OF PHYSICS AND ATMOSPHERIC SCIENCE

The undersigned hereby certify that they have read and recommend to the Faculty of Graduate Studies for acceptance a thesis entitled "**LANGEVIN EQUATION FOR DIFFUSION OF MOLECULES ADSORBED ON SURFACES**" by **Patrick Shea** in partial fulfillment of the requirements for the degree of **Master of Science**.

Dated: July 22, 2010

Supervisor: Hans-Jürgen Kreuzer

Readers: Stephen Payne

Ian Hill

DALHOUSIE UNIVERSITY

Date: **July 22, 2010**

Author: **Patrick Shea**

Title: **LANGEVIN EQUATION FOR DIFFUSION OF MOLECULES ADSORBED ON SURFACES**

Department: **Department of Physics and Atmospheric Science**

Degree: **M.Sc.** Convocation: **October** Year: **2010**

Table of Contents

List of Figures

Abstract

Starting from a classical mechanical model, a set of Langevin equations for the surface diffusion of adsorbed molecules is developed. In contrast to previous work, these Langevin equations take full account of the rotations and internal vibrations of the adsorbed molecule. These equations are then applied to a stiff dimer diffusing in one dimension, and the results compared with previous calculations for the same system. It is shown that the modifications in our new approach give significantly different results than this previous calculation, and therefore must be taken into account in future calculations for systems of this kind.

Next a new approximation method is developed by assuming that the motion of the molecule is confined to the lowest energy path between adsorption sites. This method is applicable to an arbitrarily complex molecule, and is complimentary to the first method, in that it can account for deformation of the molecule by the surface but not the internal vibrations of the molecule (whereas the first method accounts for internal vibrations but not deformation). This approximation method is then applied to a flexible dimer in two dimensions (one dimension along the surface and one perpendicular). The results are discussed and compared with those of the stiff dimer in one dimension, explaining and clarifying the difference between our results and those of previous calculations.

List of Abbreviations and Symbols Used

1D	One dimension
2D	Two dimension
a	Shape parameter in Eq. (3.1) (Ch. 3); steepness parameter in Eq. (4.27) (Ch. 4)
A	Barrier height parameter in two dimensional potential energy
$\boldsymbol{B}$	Memory-friction tensor
Dcm	Diffusion coefficient
DPA	Diffusion path approximation
E	Total energy of system
$\vec{f}_i(y)$	Curve followed by ith atom of adsorbed molecule along lowest energy diffusion path
FIM	Field ion microscopy
$\vec{g}_u^{(i)}$	Gradient of V_{MS} with respect to $\vec{u}_i$
$\boldsymbol{G}$	Transformation matrix between angular velocity and time derivative of angular coordinates for adsorbed molecule
h	Planck's constant
$\boldsymbol{H}_{uu}^{(ij)}$	Hessian matrix for potential V_S with respect to coordinates $\vec{u}_i$, $\vec{u}_j$
I_{jk}	Components of moment of inertia tensor
k_B	Boltzmann constant
k	Stiffness parameter in potential energy of dimer
$\vec{k}$	Wave vector for substrate lattice vibration
l	Lattice constant of surface
m_i	Mass of ith atom of adsorbed molecule
m_s	Mass of atoms of solid
M	Total mass of adsorbed molecule
MD	Molecular dynamics
q_k	Normal mode coordinates of substrate vibrations

$\boldsymbol{R}$	Rotation matrix for adsorbed molecule
$\vec{r}$	Center of mass position of molecule
$\vec{r}_n$	Position of nth atom of adsorbed molecule
$\vec{R}_n$	Position of nth atom of solid
$\vec{s}$	Separation vector of dimer
$\vec{s}_n$	Position of nth atom of adsorbed molecule in center of mass frame
$\vec{u}_n$	Displacement of nth atom of solid
U	Total potential energy of system
U_{eff}	Effective potential energy of adsorbed molecule
$\vec{v}_n$	Displacement of nth atom of adsorbed molecule from equilibrium in center of mass frame
V_0	Energy scale parameter in potential energy
STM	Scanning tunnelling microscopy
t	Time
T	Total kinetic energy of system (Ch. 2); temperature
T_M	Kinetic energy of adsorbed molecule
TST	Transition state theory
V_M	Internal potential energy of molecule
V_S	Internal potential energy of solid
V_{MS}	Interaction potential between adsorbed molecule and solid
V	Total potential energy of adsorbed molecule
X	Center of mass and angular coordinates for adsorbed molecule
y	Reaction coordinate
α_l	Normal mode coordinates of internal molecular vibrations
$\boldsymbol{\beta}$	Friction tensor
Γ	Hopping rate
(θ, ϕ, χ)	Euler angles describing orientation of adsorbed molecule
$\vec{\xi}$	Random force in Langevin equation
ϕ_k	Derivative of V_{MS} with respect to q_k
$\vec{\psi}$	Vector of angular coordinates for adsorbed molecule

$\vec{\omega}$	Angular velocity vector of adsorbed molecule
ω_k	Normal mode frequencies of substrate vibrations
ω_D	Debye frequency of solid
Ω_l	Normal mode frequencies of internal molecular vibrations

Chapter 1

Introduction

The diffusion of particles adsorbed on solid surfaces is important in many areas of physics. In catalysis and chemical reactions at surfaces, diffusion is essential for the reactants to find one another and is an important factor in the overall dynamics of the reaction. Crystal growth proceeds by the diffusion of atoms and atomic clusters from terraces to edge sites [1]. Diffusion of clusters on surfaces is also an essential process in surface nanostructuring [2]. An understanding of surface diffusion at a microscopic level is therefore an important step to understanding all of these phenomena.

Direct observation of surface diffusion at the level of individual atoms was first made possible in the 1960's by use of the field ion microscope (FIM) [3]. FIM experiments allow for the observation of diffusion of individual atoms as well as dimers and larger clusters, however they are limited to a few types of metal surfaces (namely platinum, rhodium, nickel, tungsten and iridium) due to the high electric fields needed for atomic imaging with helium [4].

Since these initial studies, several experimental techniques have been developed for the observation of surface diffusion, including laser ablation, helium scattering, and scanning tunneling microscopy (STM). STM allows for the tracking of individual atoms and molecules over a wide range of surfaces, and has been widely employed in surface diffusion studies (see Ref. [5] for a summary of experimental techniques).

The first step in a theoretical model of surface diffusion is a description of the interaction between the surface and the adsorbed atoms or molecules. At the most detailed level, one can perform first principles calculations of the potential energy surface. This allows for a quantitatively accurate determination of the energy barrier for diffusion for comparison with experimental data [6]. It can also provide insight into the importance of different diffusion mechanisms for a particular system, by determining which mechanism is most energetically favorable (e.g. piecewise diffusion

vs. coordinated jumps for dimers, hopping vs. exchange, etc.).

Quantitatively accurate results can also be obtained with the use of empirical potentials, such as the embedded atom method and the Rosato Guillopé Legrand potential (see Ref. [6] for a comparison of energy barriers calculated using first principles and empirical potential techniques to experimental values). These potentials consist of a sum of pairwise terms and a many-body term that accounts for the electronic interactions. The parameters in the potentials are fitted to bulk properties of the solid.

A more qualitative approach makes use of simple model potentials for the adsorbate-surface and adsorbate-adsorbate interactions. For the adsorbate-surface interaction, which must be periodic in the coordinates along the surface, the simplest choice is a cosine potential with its period equal to the lattice constant of the surface. For a more realistic description, higher Fourier components can be included [7]. Typical choices for adsorbate-adsorbate interactions are harmonic potentials [8, 9] (for stable molecules that do not dissociate) or Morse potentials [10] (when dissociation is possible). A benefit of using these simple model potentials is that analytical solutions can often be obtained, and the results can reveal general features of surface diffusion (such as, e.g., resonant diffusion of dimers [9]).

To calculate dynamical properties of the system, several different approaches have been developed. At the most detailed level, molecular dynamics (MD) simulations can be undertaken. With the use of accurate empirical potentials, MD methods can give accurate dynamical information about the system (see, e.g., Ref. [11] for calculations for the technologically important case of Si dimers on an Si surface). The inherent difficulty with MD simulations, however, is the separation of time scales of the vibrational and diffusive motion. The fastest vibrational periods are typically of the order $10^{-14}s$, while hopping times at room temperature are often of the order $1s$. The time step in the MD simulation must be comparable to the fastest vibrational periods, so direct simulation of diffusion events under experimental conditions are usually not possible. To circumvent this problem, simulations are typically done at high temperature, where the diffusion rate is much higher [4, 12].

Since typically only the motion of the adsorbed species is of interest, the problem

can be simplified by averaging over the motion of the surface atoms. In such a picture, the motion of the adsorbate is seen as Brownian motion in the periodic potential of the adsorbate-surface interaction. The trajectories of adsorbed species then satisfy a Langevin equation (equivalently, the Fokker-Planck equation describing the probability density in phase space can be used.) In the simplest approach, the adsorbate-surface interaction potential is evaluated with the surface atoms at their equilibrium positions, and the effect of the vibration of the surface atoms around their equilibrium positions is taken into account by a friction force and random stochastic force on the adsorbate. The friction coefficient is often taken as a phenomenological parameter. However, an expression for the friction can also be derived starting from a classical mechanical model [13]. In this case, a position-dependent friction tensor is obtained in terms of the interaction potential and vibrational characteristics of the substrate. This Langevin equation approach greatly simplifies the problem, resulting in a single equation of motion for the adsorbate, rather than the coupled equations for the adsorbate and surface atoms employed in MD simulations. The cost of this simplification is a less microscopically detailed view of the diffusion process.

A third approach to model the dynamics of surface diffusion is the use of lattice gas models. In lattice gas models, the surface is treated as a lattice of adsorption sites which can be either occupied or unoccupied. The hopping rate between lattice sites is used to formulate a master equation for the migration of adsorbed atoms or molecules. The hopping rates can be treated as phenomenological parameters, or calculated for a given system by a number of methods (see, e.g., Ref. [7] for a calculation of the hopping rate from a microscopic quantum mechanical model).

Transition state theory (TST) provides a simple expression for the hopping rate of an adparticle in terms of the equilibrium properties of the system. When the adparticle is localized at an adsorption site, it is trapped in a local minimum of the periodic adparticle-surface interaction, as illustrated in Fig. 1.1. In order to diffuse to a neighboring site, it must acquire enough energy to escape over the potential barrier. In TST one assumes that the adparticle is in thermal equilibrium with the surface, so that the relative probability of the adparticle being near the transition state (maximum of potential energy) is $e^{-\Delta V/k_B T}$, where ΔV is the energy barrier. Assuming a

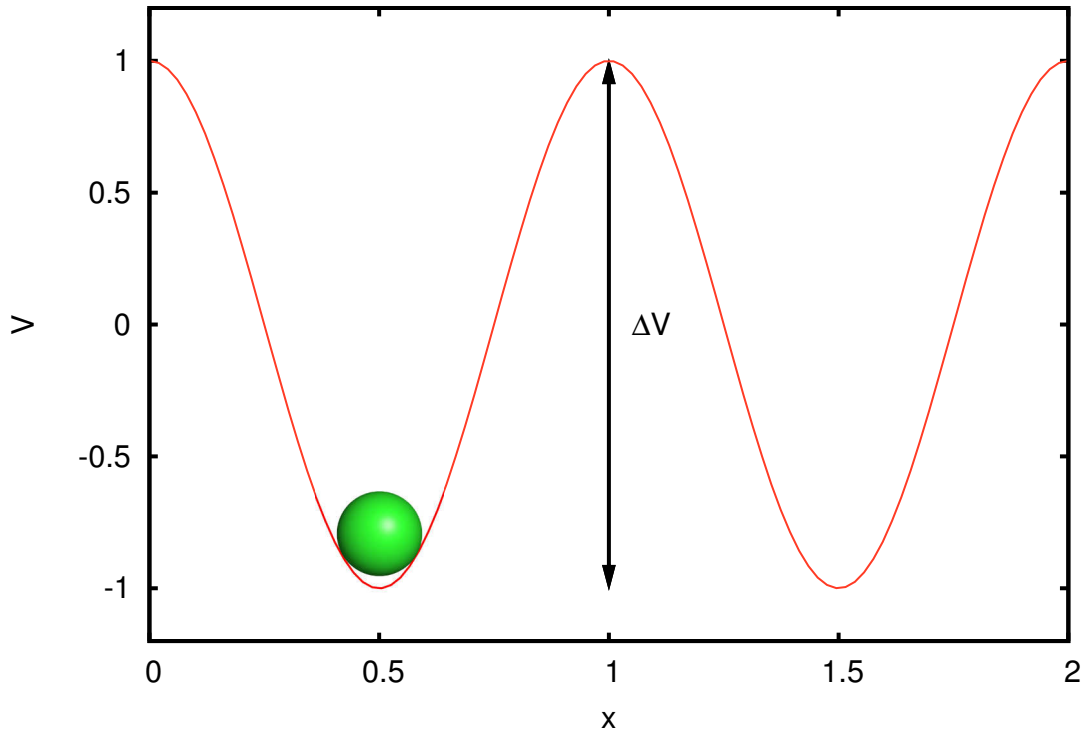

Figure 1.1: Potential energy $V(x)$ of an atom adsorbed on a surface.

Maxwell distribution for the adparticle velocity, the flux across the transition state can be found, giving the following expression for the hopping rate [14] :

$$\Gamma_{TST} = \frac{k_B T}{h} \exp(-\Delta F) = \frac{k_B T}{h} \frac{Z_t}{Z_m}, \tag{1.1}$$

where ΔF is the difference in Helmholtz free energy between the minimum and transition state, and Z_m and Z_t are the partition functions at the minimum and transition state, respectively. In the simplest approach one can use the harmonic approximation for the partition functions, giving

$$\Gamma_{TST} = \frac{1}{2\pi} \frac{\prod_i \omega_{mi}}{\prod_i \omega_{ti}} e^{-\Delta V / k_B T}, \tag{1.2}$$

where ω_{mi} and ω_{ti} are the vibration frequencies at the minimum and transition state (excluding the imaginary frequency at the transition state). Eq. (1.2) is convenient in that it gives the hopping rate entirely in terms of properties of the potential energy surface. TST is accurate when the energy barrier ΔV is large compared to the thermal energy $k_B T$, and for the intermediate friction regime, where the friction coefficient η

is of the same order as the adparticle vibration frequency, $\eta \sim \omega_m$ [15]. For stronger friction, or lower energy barriers, TST fails and a more detailed approach must be employed.

In the remainder of this chapter, we will review some general concepts related to surface diffusion which will be used throughout this thesis. We will then give a brief review of the Langevin and FP equations, and methods of solution. In chapter 2, we will derive the Langevin equation for a molecule on a surface starting from a microscopic classical mechanics model. In chapter 3 we apply the Langevin equation to the case of a dimer diffusing along a one dimensional (1D) channel. Chapter 4 deals with the diffusion path approximation (DPA), a method for the calculation of the diffusion coefficient of a multi-dimensional system in which the problem is reduced to 1D by restricting the system to the lowest energy path between adsorption sites, the position along the path being described by a reaction coordinate. We will first derive the DPA formalism, which results in a 1D Langevin equation in the 'reaction coordinate. The DPA will then be applied to the diffusion of a dimer along a 1D channel, which is also free to move in the direction perpendicular to the surface.

1.1 General Diffusion Concepts

The simplest picture of surface diffusion is that of uncorrelated hops between nearest neighbor adsorption sites. In this picture, the adparticle performs a random walk across the surface, and the probability of the ith site being occupied is governed by the following master equation (in 1D):

$$\frac{\partial \rho_i}{\partial t} = \Gamma_{\rightarrow}\rho_{i-1} + \Gamma_{\leftarrow}\rho_{i+1} - (\Gamma_{\rightarrow} + \Gamma_{\leftarrow})\rho_i, \tag{1.3}$$

where $\Gamma_{\rightarrow}$ and $\Gamma_{\leftarrow}$ are the hopping rates for an adparticles to move to the right or left. For an isotropic surface, there should be equal probability for a hop to the left or right, so $\Gamma_{\rightarrow} = \Gamma_{\leftarrow} = \Gamma/2$, where Γ is the total hopping rate. If we now take the probability to be a slowly varying smooth function of position, $\rho_i = \rho(x_i)$, then we

can expand $\rho(x)$ in a Taylor series, so that (1.3) becomes

$$\begin{aligned}\frac{\partial\rho}{\partial t} &= \frac{\Gamma}{2}\left[-2\rho + \left(\rho + l\frac{\partial\rho}{\partial x} + \frac{l^2}{2}\frac{\partial^2\rho}{\partial x^2}\right) + \left(\rho - l\frac{\partial\rho}{\partial x} + \frac{l^2}{2}\frac{\partial^2\rho}{\partial x^2}\right)\right] \\ &= \frac{\Gamma l^2}{2}\frac{\partial^2\rho}{\partial x^2},\end{aligned} \tag{1.4}$$

where l is the jump distance (equal to the lattice constant in this simple picture). This is a diffusion equation of the form $\dot{\rho} = D\rho''$, with diffusion coefficient $D = \Gamma l^2/2$. When hops to sites further than the nearest neighbor are allowed, and the adparticle can diffuse in more than one dimension, the relationship generalizes to [16]

$$D = \frac{\Gamma\langle l^2\rangle}{2d}, \tag{1.5}$$

where d is the number of dimensions, and $\langle l^2\rangle$ is the mean square jump distance.

In the cases of low barriers or weak frictional damping, long jumps become important to the diffusive motion [15,17,18], and calculation of the average jump length can be difficult. Furthermore, there will in the general case be correlations between successive jumps, so that there must be corrections to the random walk formula (1.5). A more general definition of the diffusion coefficient is therefore needed.

When the trajectories of individual particles are followed (as in STM or FIM experiments), the appropriate quantity is the tracer diffusion coefficient, defined as

$$D = \lim_{t\to\infty}\frac{\langle\vec{r}^2\rangle}{2t}, \tag{1.6}$$

where $\vec{r}$ is the position of the adparticle. This relation can easily be verified for the above simple case by making use of the mean square displacement for a random walk in 1D, $\langle x^2\rangle = Nl^2$, where $N = \Gamma t$ is the number of steps. Eq. (1.6) allows a calculation of the diffusion coefficient from the average long time behavior of the adparticle, which in the following chapters we will calculate via a Langevin equation. In practice, this is also typically how diffusion coefficients are measured in experiments; an average of the displacement of an adparticle over many trials is taken.

1.2 Langevin Equation

As we will show in the next chapter, in the most general case an adparticle obeys the following generalized Langevin equation for its position $\vec{r}$

$$M\ddot{\vec{r}} + \int_0^t \boldsymbol{B}[\vec{r}(t), \vec{r}(t'), t-t'] \cdot \dot{\vec{r}}(t')dt' + \nabla V = \vec{\xi}(\vec{r}, t). \tag{1.7}$$

V is the interaction potential between the adparticle and the surface with all of the surface atoms fixed at their lattice positions. The friction-memory tensor $\boldsymbol{B}$, and the random force $\vec{\xi}$ account for the vibration of the surface atoms around their lattice positions; that is, they account for the coupling of the adparticle to the phonons in the solid. This phonon coupling is the mechanism by which the adparticle exchanges energy with the solid, and attains enough energy to diffuse to a neighboring adsorption site. There will also be coupling between the electronic degrees of freedom, which is not accounted for in the classical mechanics approach used to derive Eq. (1.7). However, for many systems (particularly physisorbed systems), this coupling is negligible compared to the coupling to the phonons [16, 19].

The random force and friction-memory tensor are related by the fluctuation-dissipation theorem [20, 21],

$$\langle \vec{\xi}(\vec{r}(t), t)\vec{\xi}(\vec{r}(t'), t')\rangle = k_B T \boldsymbol{B}[\vec{r}(t), \vec{r}(t'), t-t']. \tag{1.8}$$

In most systems of interest, the time scale for diffusion is very long compared to the fast vibrational motion of the surface atoms, and the random force is uncorrelated in time, $\langle \vec{\xi}(t)\vec{\xi}(t')\rangle \sim \delta(t-t')$. Then Eq. (1.7) simplifies to a standard Langevin equation,

$$M\ddot{\vec{r}} + \boldsymbol{\beta} \cdot \dot{\vec{r}} + \nabla V = \vec{\xi}, \tag{1.9}$$

where $\langle \vec{\xi}(\vec{r}(t), t)\vec{\xi}(\vec{r}(t'), t')\rangle = 2k_B T \boldsymbol{\beta}\delta(t-t')$. It can be shown that Eq. (1.9) is equivalent to the following equation for the probability density in phase space $\rho(\vec{r}, \vec{v})$, called the Fokker-Planck, or Klein-Kramers equation [20, 21]

$$\frac{\partial \rho}{\partial t} + \vec{v} \cdot \nabla_r \rho - \frac{\nabla_r V}{M} \cdot \nabla_v \rho = \nabla_v \cdot \frac{\boldsymbol{\beta}}{M} \cdot \left(\vec{v}\rho + \frac{k_B T}{M} \nabla_v \rho \right), \tag{1.10}$$

where ∇_v is the gradient in velocity space, and ∇_r is the gradient in position space. The terms in this equation have the following interpretations. The left hand side is simply the hydrodynamic derivative of the probability, $\frac{D\rho}{Dt}$. The second term is a convective term in position space due to the velocity $\vec{v}$, and the third term is a convective term in velocity space due to the force $-\nabla_r V$. The right hand side is a source term that comes from the interaction of the adparticle with the phonons.

To solve for the behavior of the adparticle in this approach, two basic methods are widely employed. Firstly, the Langevin equation (1.9) can be integrated numerically for a particular realization of the random force, and the results averaged over many realizations [8, 17, 22]. Secondly, the Fokker-Planck equation (1.10) can be solved numerically using the matrix continued fraction method (MCFM) [21,23]. In 1D, the MCFM provides a very accurate and efficient solution to the Fokker-Planck equation for the moderate to high friction regimes; for low friction, and also for very high barriers the computation time requires becomes much higher. In 2D the MCFM becomes much more complicated [23], and for three or more dimensions it becomes practically intractable [16].

In addition to these methods, there are also analytical expressions for the diffusion coefficient or hopping rate available in several limiting cases. For high barriers $\Delta V \gg k_B T$, where only nearest neighbor hops are important, the hopping rate is given by the following expression for the moderate to high friction regime [24, 25]

$$\Gamma = \Gamma_{TST}\left(\sqrt{1+\frac{\eta^2}{4\bar{\omega}_s^2}}-\frac{\eta}{2\bar{\omega}_s}\right), \tag{1.11}$$

assuming a constant friction coefficient $\beta = M\eta$. $\bar{\omega}_s$ is the unstable vibration frequency at the transition state, and Γ_{TST} is given in Eq. (1.1). For the low to moderate friction regime, the hopping rate is given by [26]

$$\Gamma = \Gamma_{TST}\exp\left[\frac{1}{\pi}\int_0^\infty du \frac{\ln\left\{1-\exp\left[-\frac{4\eta\Delta V}{\omega_0 k_B T}\left(u^2+\frac{1}{4}\right)\right]\right\}}{u^2+\frac{1}{4}}\right]. \tag{1.12}$$

This expression is only valid in one dimension.

For barriers of arbitrary height there are analytical results for the diffusion coefficient in both the low friction and high friction regimes, in 1D. For low friction, the

following expression holds [21]

$$D = \frac{\pi k_B T}{2M\eta} e^{-\Delta V/k_B T}. \tag{1.13}$$

This expression is only accurate when the friction is very small, which is typically not the case in surface diffusion. In the high friction regime, the diffusion coefficient is given by [27]

$$D = k_B T \left[\frac{1}{l} \int_0^l \beta(x) e^{V_{MS}(x)/k_B T} dx \frac{1}{l} \int_0^l e^{-V_{MS}(x')/k_B T} dx' \right]^{-1}. \tag{1.14}$$

We will make use of this expression in the following chapters to calculate the diffusion coefficient for a dimer in 1D.

Chapter 2

Derivation of Langevin Equation

In this chapter we derive the Langevin equation for a molecule adsorbed on a surface starting from a classical mechanical model of a molecule and surface made up of point particles interacting via local potentials. A classical mechanics model is appropriate when the adsorbate is heavy enough so that quantum effects are negligible. This is the case for most systems of interest, with an exception being hydrogen on metal surfaces, where quantum tunneling effects become important at low temperatures [28].

In deriving the Langevin equation, we follow the work of Tsekov and Ruckenstein. In Ref. [13], they derived a Langevin equation for adatoms coupled to the phonons of a solid. After reviewing their derivation, we will extend the formalism to include coupling of the center of mass motion of a molecule to the internal vibrational degrees of freedom.

2.1 Interacting Atoms

We first review the derivation of Ref. [13] for a system of interacting atoms (which can either be bound in a molecule or free). Consider a system of atoms adsorbed on a surface. We denote the positions of the atoms of the solid by $\vec{R}_i$, and those of the adsorbed atoms by $\vec{r}_i$. To account for the vibrations of the substrate atoms, we write

$$\vec{R}_i = \vec{R}_i^{(0)} + \vec{u}_i, \tag{2.1}$$

where $\vec{u}_i$ is the deviation from the equilibrium position $\vec{R}_i^{(0)}$.

The kinetic energy can then be written as

$$T = \sum_i \frac{1}{2} m_s |\dot{\vec{R}}_i|^2 + \sum_i \frac{1}{2} m_i |\dot{\vec{r}}_i|^2 \tag{2.2}$$

$$= \sum_i \frac{1}{2} m_s |\dot{\vec{u}}_i|^2 + \sum_i \frac{1}{2} m_i |\dot{\vec{r}}_i|^2, \tag{2.3}$$

where m_s is the mass of the lattice atoms and m_i is the mass of the ith adsorbed atom. The potential energy can be split into three terms: the potential energy of the free solid (in the absence of the molecule) V_S, the interaction energy of the adatoms with each other V_M, and the interaction energy of the adatoms with the surface V_{MS},

$$U = V_S(\{\vec{R}_n\}) + V_M(\{\vec{r}_n\}) + V_{MS}(\{\vec{R}_n\}, \{\vec{r}_n\}). \tag{2.4}$$

We now treat the phonons in the harmonic approximation by expanding V_S and V_{MS} to lowest order in the displacements $\vec{u}_i$,

$$V_S = V_S^{(0)} + \frac{1}{2}\sum_{i,j} \vec{u}_i \cdot \left(\nabla_{R_i}\nabla_{R_j} V_S\right)^{(0)} \cdot \vec{u}_j, \tag{2.5}$$

$$V_{MS} = V_{MS}^{(0)} + \sum_i \left(\nabla_{R_i} V_{MS}\right)^{(0)} \cdot \vec{u}_i, \tag{2.6}$$

where the (0) superscript denotes quantities evaluated at $\vec{u}_i = 0$. We have assumed only a linear coupling of the adatoms to the phonons, neglecting the second order terms in V_{MS}. The second order terms correspond to two-phonon collisions, which have been shown to be negligible in typical systems [29]. We then write the full potential as

$$\begin{aligned} U = V_S^{(0)} + V_M(\{\vec{r}_n\}) + V_{MS}^{(0)}(\{\vec{r}_n\}) + \sum_i \vec{g}_u^{(i)}(\{\vec{r}_n\}) \cdot \vec{u}_i \\ + \sum_{i,j} \vec{u}_i \cdot \boldsymbol{H}_{uu}^{(ij)} \cdot \vec{u}_j, \end{aligned} \tag{2.7}$$

where

$$\vec{g}_u^{(i)} = \left(\nabla_{R_i} V_{MS}\right)^{(0)} = \left(\nabla_{u_i} V_{MS}\right)^{(0)} \tag{2.8}$$

$$\boldsymbol{H}_{uu}^{(ij)} = \left(\nabla_{R_i}\nabla_{R_j} V_S\right)^{(0)} = \left(\nabla_{u_i}\nabla_{u_j} V_S\right)^{(0)}. \tag{2.9}$$

The total energy $T + U$ can be rewritten in terms of the normal mode frequencies ω_k and coordinates q_k (which we take to be complex) of the solid vibrations to give

$$\begin{aligned} E = T + U = \sum_i \frac{1}{2} m_i |\dot{\vec{r}}_i|^2 + \sum_k \frac{1}{2}|\dot{q}_k|^2 + V_S^{(0)} + V_M(\{\vec{r}_n\}) + V_{MS}^{(0)}(\{\vec{r}_n\}) \\ + \sum_k \phi_k(\{\vec{r}_n\}) q_k + \sum_k \frac{1}{2}\omega_k^2 |q_k|^2, \end{aligned} \tag{2.10}$$

where

$$\phi_k = \left(\frac{\partial V_{MS}}{\partial q_k}\right)^{(0)}. \tag{2.11}$$

The equations of motion for $\vec{r}_i$ and q_k can be found from the Euler-Lagrange equations, giving

$$m_i\ddot{\vec{r}}_i + \nabla_{r_i}(V_M + V_{MS}^{(0)}) + \sum_k q_k \nabla_{r_i}\phi_k = 0 \tag{2.12}$$

$$\ddot{q}_k + \omega_k^2 q_k + \phi_k^* = 0. \tag{2.13}$$

The equations for q_k are simply uncoupled driven harmonic oscillators, which can be solved analytically. By substituting the solutions into Eq. (2.12) we will obtain a set of Langevin equations for the adatom positions $\vec{r}_i$. Eqs. (2.13) have the solutions

$$q_k(t) = q_k(0)\cos(\omega_k t) + \frac{1}{\omega_k}\dot{q}_k(0)\sin(\omega_k t) - \frac{1}{\omega_k}\int_0^t \sin[\omega_k(t-t')]\phi_k^*(\{\vec{r}_n(t')\})dt'. \tag{2.14}$$

To make Eq. (2.12) take the form of a Langevin equation, we must rewrite (2.14) using integration by parts,

$$\begin{aligned} q_k(t) = &\left[q_k(0) + \frac{1}{\omega_k}\phi_k^*(\{\vec{r}_n(0)\})\right]\cos(\omega_k t) + \frac{1}{\omega_k}\dot{q}_k(0)\sin(\omega_k t) - \frac{1}{\omega_k^2}\phi_k^*(\{\vec{r}_n(t)\}) \\ &+ \frac{1}{\omega_k^2}\int_0^t \cos[\omega_k(t-t')]\sum_j \nabla_{r_j}\phi_k^*(\{\vec{r}_n(t')\})\cdot\dot{\vec{r}}_j(t')dt'. \end{aligned} \tag{2.15}$$

Making use of these solutions, Eq. (2.12) becomes

$$m_i\ddot{\vec{r}}_i + \sum_j \int_0^t \boldsymbol{B}_{ij}\cdot\dot{\vec{r}}_j(t')dt' + \nabla_{r_i}U_{\text{eff}} = \vec{\xi}_i, \tag{2.16}$$

where

$$\boldsymbol{B}_{ij}[\{\vec{r}_n(t)\},\{\vec{r}_n(t')\},t-t'] = \sum_k \frac{\cos[\omega_k(t-t')]}{\omega_k^2}\nabla_{r_i}\phi_k(\{\vec{r}_n(t)\})\nabla_{r_j}\phi_k^*(\{\vec{r}_n(t')\}), \tag{2.17}$$

$$U_{\text{eff}} = V_M + V_{MS}^{(0)} - \frac{1}{2}\sum_k \frac{|\phi_k|^2}{\omega_k^2}, \tag{2.18}$$

$$\begin{aligned} \vec{\xi}_i(\{\vec{r}_n(t)\},t) = -\sum_k &\left[\left(q_k(0) + \frac{\phi_k^*(\{\vec{r}_n(0)\})}{\omega_k^2}\right)\cos(\omega_k t) + \frac{\dot{q}_k(0)}{\omega_k}\sin(\omega_k t)\right] \\ &\times \nabla_{r_i}\phi_k(\{\vec{r}_n(t)\}). \end{aligned} \tag{2.19}$$

This is a set of generalized Langevin equations for the adatoms, so called because of the presence of the second term on the left hand side of Eq. (2.16). This is a memory term, involving an integral over the entire past history of the system; a standard Langevin equation has a friction term, proportional only to the velocity at time t, $\dot{\vec{r}}_i(t)$, with no memory effects.

The force $\vec{\xi}_i$ on the right-hand side of Eq. (2.16) is a random stochastic force. The stochastic nature of $\vec{\xi}_i$ comes from its dependence on the initial conditions $q_k(0), \dot{q}_k(0)$, which we denote collectively by Γ. Assuming the system is initially in thermal equilibrium the probability of a set of initial conditions is given by

$$\rho(\Gamma) = \frac{1}{Z} e^{-E_\Gamma/k_B T}, \tag{2.20}$$

where $E_\Gamma = \sum_k (|\dot{q}_k(0)|^2/2 + \omega_k^2 |q_k(0)|^2/2)$, and $Z = \int d\Gamma e^{-E_\Gamma/k_B T}$ is the partition function. The average of a quantity $A(\Gamma)$ is then given by

$$\langle A \rangle = \frac{1}{Z} \int d\Gamma A(\Gamma) \rho(\Gamma). \tag{2.21}$$

Using this averaging procedure, it is easy to show that the average force is zero,

$$\langle \vec{\xi}_i(\{\vec{r}_n\}, t) \rangle = 0, \tag{2.22}$$

as expected for a Langevin force [20, 21].

The memory term and random force both arise from interaction of the ad-atoms with the phonons, and they are related by the fluctuation-dissipation theorem [20, 21]

$$\langle \vec{\xi}_i(\{\vec{r}_n(t)\}, t) \vec{\xi}_j(\{\vec{r}_n(t')\}, t') \rangle = k_B T \boldsymbol{B}_{ij}[\{\vec{r}_n(t)\}, \{\vec{r}_n(t')\}, t - t'], \tag{2.23}$$

which can be verified by making use of Eqs. (2.19) and (2.17). The memory term therefore arises from the finite time correlations of the random force. In a standard Langevin equation, the random force is completely uncorrelated in time, $\langle \vec{\xi}(t) \vec{\xi}(t') \rangle \sim \delta(t - t')$, so the integral in the memory term disappears, and a simple friction term is recovered.

The last term on the left-hand side of Eq.(2.16) is the so-called adiabatic potential [16]. It is simply the potential energy averaged over the positions of the substrate atoms; i.e. the configurational free energy,

$$U_{\text{eff}}(\{\vec{r}_n\}) = \langle U(\{\vec{r}_n\}, \Gamma) \rangle, \tag{2.24}$$

which can be verified by using Eq. (2.7) for the potential energy.

2.2 Stable Molecules

For the rest of this chapter, we consider the system of the previous section with the additional constraint that the adatoms form a stable molecule whose atoms make small deviations from their equilibrium positions (with respect to the molecule center of mass). What follows in the remainder of this chapter is new work.

To describe the motion of the molecule, we consider a reference frame that rotates with the molecule, and has its origin at the molecule's center of mass $\vec{r} = \frac{1}{M}\sum_i m_i \vec{r}_i$ (where $M = \sum_i m_i$ is the total mass of the molecule). The orientation of this frame with respect to the lab frame is given by three angles, denoted by $\vec{\psi}$. The positions of the atoms in the rotating center of mass frame are denoted as $\vec{s}_i$, and the positions in the lab frame are related by

$$\vec{r}_i = \vec{r} + \boldsymbol{R}^{-1}(\vec{\psi})\vec{s}_i, \tag{2.25}$$

where $\boldsymbol{R}(\vec{\psi})$ is a rotation matrix. If we take the angles to be the Euler angles, $\vec{\psi} = (\theta, \phi, \chi)$, (as defined in Ref. [30]) the rotation matrix is

$$\boldsymbol{R} = \begin{pmatrix} \cos\theta\cos\phi\cos\chi - \sin\phi\sin\chi & \cos\theta\sin\phi\cos\chi + \cos\phi\sin\chi & -\sin\theta\cos\chi \\ -\cos\theta\cos\phi\cos\chi - \sin\phi\cos\chi & \cos\theta\sin\phi\cos\chi + \cos\phi\sin\chi & \sin\theta\sin\chi \\ \sin\theta\cos\phi & \sin\theta\sin\phi & \cos\theta \end{pmatrix}. \tag{2.26}$$

Note that the positions in the center of mass frame, $\vec{s}_i$, are not all independent, since the center of mass coordinate $\vec{r}$ and the angles $\vec{\psi}$ have already been specified. For an N-atom molecule, there will be $3N-6$ internal coordinates ($3N-5$ for a linear molecule), so 6 conditions must be satisfied by the coordinates $\vec{s}_i$. Three of these have already been specified, namely that the center of mass in the moving frame must be zero,

$$\sum_i m_i \vec{s}_i = 0. \tag{2.27}$$

The other set of conditions can be taken to be

$$\sum_i m_i \vec{s}_i^{(0)} \times \vec{v}_i = 0, \tag{2.28}$$

where $\vec{s}_i^{(0)}$ and $\vec{v}_i$ are defined by $\vec{s}_i = \vec{s}_i^{(0)} + \vec{v}_i$ and $\vec{s}_i = \vec{s}_i^{(0)}$ gives the equilibrium configuration of the molecule. The condition (2.28) is approximately equivalent to setting the angular momentum in the rotating frame equal to zero, as long as the displacements $\vec{v}_i$ are small [31].

Following Ref. [30], we write the kinetic energy of the adsorbed molecule in terms of the center of mass and internal coordinates:

$$T_M = \sum_i \frac{1}{2} m_i |\dot{\vec{r}}_i|^2 = \sum_i \frac{1}{2} m_i |\dot{\vec{r}} + \boldsymbol{R}^{-1}(\vec{\psi})\dot{\vec{s}}_i + \dot{\boldsymbol{R}}^{-1}(\vec{\psi})\vec{s}_i|^2. \tag{2.29}$$

Writing the above in matrix notation, and using the fact that $\boldsymbol{R}^{-1} = \boldsymbol{R}^T$ for rotation matrices (where the superscript T denotes the transpose),

$$\begin{aligned} T_M &= \sum_i \frac{1}{2} m_i \left(\dot{\vec{r}}^T + \dot{\vec{s}}_i^T \boldsymbol{R} + \vec{s}_i^T \dot{\boldsymbol{R}} \right) \left(\dot{\vec{r}} + \boldsymbol{R}^T \dot{\vec{s}}_i + \dot{\boldsymbol{R}}^T \vec{s}_i \right) \\ &= \frac{1}{2} M \dot{\vec{r}}^T \dot{\vec{r}} + \dot{\vec{r}}^T \left(\boldsymbol{R}^T \sum_i m_i \dot{\vec{s}}_i + \dot{\boldsymbol{R}}^T \sum_i m_i \vec{s}_i \right) + \sum_i \frac{1}{2} m_i \dot{\vec{s}}_i^T \dot{\vec{s}}_i \\ &\quad + \sum_i m_i \dot{\vec{s}}_i^T \boldsymbol{R} \dot{\boldsymbol{R}}^T \vec{s}_i + \sum_i \frac{1}{2} m_i (\vec{s}_i^T \dot{\boldsymbol{R}} \boldsymbol{R}^T)(\boldsymbol{R} \dot{\boldsymbol{R}}^T \vec{s}_i). \end{aligned} \tag{2.30}$$

The two terms in the brackets are both zero, since they involve the center of mass of the molecule in the rotated center of mass frame (which is zero by definition).

The kinetic energy can be rewritten in terms of the angular velocity $\vec{\omega}$ of the molecule in the following way. First, note that since the rotation matrix is orthogonal, $\boldsymbol{R}\boldsymbol{R}^T = \mathbf{1}$ (where $\mathbf{1}$ is the identity matrix). Differentiating with respect to t gives $\boldsymbol{R}\dot{\boldsymbol{R}}^T = -\boldsymbol{R}^T\dot{\boldsymbol{R}}$, so the matrix $\boldsymbol{R}\dot{\boldsymbol{R}}^T$ is antisymmetric, and it can be shown [31] that its elements are

$$\boldsymbol{R}\dot{\boldsymbol{R}}^T = \begin{pmatrix} 0 & -\omega_z & \omega_y \\ \omega_z & 0 & -\omega_x \\ -\omega_y & \omega_x & 0 \end{pmatrix}, \tag{2.31}$$

where ω_i are the components of $\vec{\omega}$ in the rotated coordinate system. The matrix product $\boldsymbol{R}\dot{\boldsymbol{R}}^T \vec{s}_i$ can then be written as a vector cross product,

$$\boldsymbol{R}\dot{\boldsymbol{R}}^T \vec{s}_i = \vec{\omega} \times \vec{s}_i, \tag{2.32}$$

and the kinetic energy becomes

$$T_M = \frac{1}{2}M|\dot{\vec{r}}|^2 + \sum_i \frac{1}{2}m_i|\vec{\omega}\times\vec{s}_i|^2 + \sum_i \frac{1}{2}m_i|\dot{\vec{s}}_i|^2 + \sum_i m_i(\vec{\omega}\times\vec{s}_i)\cdot\dot{\vec{s}}_i. \tag{2.33}$$

The second term can be written in terms of the moment of inertia tensor in the following way

$$\begin{aligned} m_i|\vec{\omega}\times\vec{s}_i|^2 &= m_i\varepsilon_{jkl}\omega_k s_{il}\varepsilon_{jmn}\omega_m s_{in} = m_i(\delta_{km}\delta_{ln}-\delta_{kn}\delta_{lm})s_{il}s_{in}\omega_k\omega_m \\ &= m_i(s_{il}s_{il}\delta_{km}-s_{ik}s_{im})\omega_k\omega_m, \end{aligned} \tag{2.34}$$

where the Einstein summation notation is used, and s_{ij} is the jth component of $\vec{s}_i$. The kinetic energy can then be written

$$\begin{aligned} T_M &= \frac{1}{2}M|\dot{\vec{r}}|^2 + \sum_{jk}\frac{1}{2}I_{jk}\omega_j\omega_k + \sum_i \frac{1}{2}m_i|\dot{\vec{s}}_i|^2 + \sum_i m_i(\vec{\omega}\times\vec{s}_i)\cdot\dot{\vec{s}}_i \\ &= \frac{1}{2}M|\dot{\vec{r}}|^2 + \sum_{jk}\frac{1}{2}I_{jk}\omega_j\omega_k + \sum_i \frac{1}{2}m_i|\dot{\vec{v}}_i|^2 + \vec{\omega}\cdot\sum_i m_i(\vec{v}_i\times\dot{\vec{v}}_i), \end{aligned} \tag{2.35}$$

where the last term has been rewritten using the identity $\vec{a}\cdot(\vec{b}\times\vec{c}) = \vec{b}\cdot(\vec{a}\times\vec{c})$ and the condition (2.28), and I_{jk} are the elements of the moment of inertia tensor,

$$I_{jk} = \sum_i m_i(|\vec{s}_i|^2\delta_{jk} - s_{ij}s_{ik}). \tag{2.36}$$

If we define the axes of the rotating reference frame so that they coincide with the principle axes of inertia for the molecule, then the off diagonal elements of I_{jk} vanish, and we have

$$T_M = \frac{1}{2}M|\dot{\vec{r}}|^2 + \sum_j \frac{1}{2}I_{jj}\omega_j^2 + \sum_i \frac{1}{2}m_i|\dot{\vec{v}}_i|^2 + \vec{\omega}\cdot\sum_i m_i(\vec{v}_i\times\dot{\vec{v}}_i), \tag{2.37}$$

We now change coordinates from the displacements $\vec{v}_i$ to the normal coordinates α_k, related by a linear transformation, $\sqrt{m_i}v_{i,j} = \sum_k l^k_{i,j}\alpha_k$, where $v_{i,j}$ is the jth component of $\vec{v}_i$. The kinetic energy then reads

$$T_M = \frac{1}{2}M|\dot{\vec{r}}|^2 + \sum_j \frac{1}{2}I_{jj}\omega_j^2 + \sum_i \frac{1}{2}\dot{\alpha}_i^2 + \sum_{ijk}\omega_i\zeta^i_{jk}\alpha_j\dot{\alpha}_k, \tag{2.38}$$

where ζ^i_{jk} are the Coriolis parameters, defined as

$$\zeta^i_{jk} = \sum_{mnp}\varepsilon_{imn}l^j_{p,m}l^k_{p,n}. \tag{2.39}$$

The kinetic energy has the form $T_M = T_{\text{trans}} + T_{\text{rot}} + T_{\text{vib}} + T_{\text{cor}}$. The first term is the translational kinetic energy, the second is the kinetic energy of overall rotation of a rigid molecule, the third is the vibrational energy of a non-rotating molecule, and the fourth term, called the Coriolis energy, accounts for the coupling between the rotational and vibrational motion. There will also be coupling between the rotational and vibrational motions due to the dependence of the moment of inertia tensor I_{jk} on the normal coordinates α_k. However, if the displacements of the atoms from their equilibrium positions $\vec{s}_i^{(0)}$ are small, α_k will be small and $T_{\text{cor}} \sim \alpha_j \dot{\alpha}_k$ will therefore be negligible compared to $T_{\text{vib}} \sim \dot{\alpha}_k^2$, and the dependence of the moment of inertia tensor on α_k can also be neglected. This approximation, known as the rigid rotor approximation, will decouple the rotational and vibrational motion, and allow us to derive a set of Langevin equations for the semi-rigid molecule.

We must make one further modification to the expression for the kinetic energy. In order to apply the Euler-Lagrange equations and obtain equations of motion for the molecule, we must write T_M in terms of time derivatives of the angles $\vec{\psi}$, rather than the angular velocity $\vec{\omega}$. $\vec{\omega}$ is related to the time derivatives of the angles ψ_i by

$$\vec{\omega} = \boldsymbol{G}\dot{\vec{\psi}}, \tag{2.40}$$

where

$$\boldsymbol{G} = \begin{pmatrix} \sin\chi & -\sin\theta\cos\chi & 0 \\ \cos\chi & \sin\theta\sin\chi & 0 \\ 0 & \cos\theta & 1 \end{pmatrix}. \tag{2.41}$$

Making use of this relation, along with the rigid rotor approximation, the kinetic energy can be written as

$$\begin{aligned} T_M &= \frac{1}{2}M|\dot{\vec{r}}|^2 + \sum_i \frac{1}{2} I_{ii} \sum_{jk} \boldsymbol{G}_{jk}\dot{\psi}_j\dot{\psi}_k + \sum_i \frac{1}{2}\dot{\alpha}_i^2 \\ &= \frac{1}{2}M|\dot{\vec{r}}|^2 + \sum_{jk} U_{jk}\dot{\psi}_j\dot{\psi}_k + \sum_i \frac{1}{2}\dot{\alpha}_i^2, \end{aligned} \tag{2.42}$$

where

$$U_{jk} = \sum_i I_{ii}\boldsymbol{G}_{ij}\boldsymbol{G}_{ik}. \tag{2.43}$$

We can now make use of Eq. (2.42) to obtain the equations of motion for the adsorbed molecule. The total kinetic energy is

$$T = \frac{1}{2}M|\dot{\vec{r}}|^2 + \sum_{jk} U_{jk}\dot{\psi}_j\dot{\psi}_k + \sum_l \frac{1}{2}|\dot{\alpha}_l|^2 + \sum_k \frac{1}{2}|\dot{q}_k|^2. \tag{2.44}$$

We also expand the molecular potential V_M and the interaction potential V_{MS}. in the normal coordinates, giving

$$V_M = V_M^{(0)} + \sum_l \frac{1}{2}\Omega_l^2\alpha_l^2, \tag{2.45}$$

$$V_{MS} = V_{MS}^{(0)}(X) + \sum_k \phi_k(X)q_k + \sum_l \Theta_l(X)\alpha_l, \tag{2.46}$$

where Ω_l are the normal mode frequencies of the internal molecular vibrations, X stands for the center of mass coordinates $\vec{r}$ and angle coordinates $\vec{\psi}$, and

$$\Theta_l = \left(\frac{\partial V_{MS}}{\partial \alpha_l}\right)^{(0)}. \tag{2.47}$$

Following the same procedure as in the previous section, we obtain a set of Langevin equations for the molecule. Instead of an equation for each atom, we obtain only two equations: one for the center of mass motion, and one for the rotational motion. The center of mass equation reads

$$M\ddot{\vec{r}} + \int_0^t \left[\boldsymbol{B}_{rr}\cdot\dot{\vec{r}}(t') + \boldsymbol{B}_{r\psi}\cdot\dot{\vec{\psi}}(t')\right]dt' + \nabla_r U_{\text{eff}}(X) = \vec{\xi}_r(X,t), \tag{2.48}$$

and the equation for the rotational motion is

$$\boldsymbol{U}\ddot{\vec{\psi}} + \sum_{jk}\vec{\gamma}_{jk}\dot{\psi}_j\dot{\psi}_k + \int_0^t \left[\boldsymbol{B}_{\psi r}\cdot\dot{\vec{r}}(t') + \boldsymbol{B}_{\psi\psi}\cdot\dot{\vec{\psi}}(t')\right]dt' + \nabla_\psi U_{\text{eff}}(X) = \vec{\xi}_\psi(X,t), \tag{2.49}$$

where the elements of $\vec{\gamma}_{jk}$ are

$$\gamma_{jk,i} = \frac{\partial U_{ik}}{\partial \psi_j} - \frac{1}{2}\frac{\partial U_{jk}}{\partial \psi_i}. \tag{2.50}$$

The memory-friction and random force are given by

$$\begin{aligned}\boldsymbol{B}_{ab}[X(t),X(t'),t-t'] &= \sum_k \frac{\cos[\omega_k(t-t')]}{\omega_k^2}\nabla_a\phi_k^*(X(t))\nabla_b\phi_k(X(t')) \\ &\quad + \sum_l \frac{\cos[\Omega_l(t-t')]}{\Omega_l^2}\nabla_a\Theta_l(X(t))\nabla_b\Theta_l(X(t')),\end{aligned} \tag{2.51}$$

$$\begin{aligned}\vec{\xi}_a(X,t) = &-\sum_k\left[\left(q_k(0)+\frac{\phi_k(X(0))}{\omega_k^2}\right)\cos(\omega_k t)+\frac{\dot{q}_k(0)}{\omega_k}\sin(\omega_k t)\right]\nabla_a\phi_k(X) \\ &-\sum_l\left[\left(\alpha_l(0)+\frac{\Theta_l(X(0))}{\Omega_l^2}\right)\cos(\Omega_l t)+\frac{\dot{\alpha}_l(0)}{\Theta_l}\sin(\Omega_l t)\right]\nabla_a\Theta_l(X),\end{aligned} \tag{2.52}$$

where a, b stands for either r or ψ. The effective potential is

$$U_{\text{eff}}(X) = \langle U(X,\Gamma)\rangle = V_{MS}^{(0)}(X) - \frac{1}{2}\sum_k\frac{|\phi_k(X)|^2}{\omega_k^2} - \frac{1}{2}\sum_l\frac{\Theta_l^2(X)}{\Omega_l^2}. \tag{2.53}$$

Usually one or more of the angular degrees of freedom of the adsorbed molecule will be confined to small oscillations. For example, a large planar molecule will typically only make rotations through an axis perpendicular to the surface [32–34]. A molecule diffusing along a 1D channel will not make any rotations. In these cases the angles through which the molecule only makes small rotations may be treated in the harmonic approximation, and will add to the other normal modes of the molecule α_i. For a molecule that only rotates through an axis perpendicular to the surface, the angular equation (2.49) simplifies substantially to

$$I_{zz}\ddot{\chi} + \int_0^t\left[\vec{B}_{\chi r}\cdot\dot{\vec{r}}(t') + B_{\chi\chi}\dot{\chi}(t')\right]dt' + \frac{\partial}{\partial\chi}U_{\text{eff}}(X) = \xi_\chi(X,t), \tag{2.54}$$

where $\vec{B}_{\chi r}$,$B_{\chi\chi}$ and ξ_χ are given by Eqs. (2.51) and (2.52) with ∇_ψ replaced by $\frac{\partial}{\partial\chi}$.

The generalized Langevin equations derived so far in this chapter are quite complicated to solve in general, due to the memory terms. However, in the surface diffusion systems we wish to study, memory effects are typically negligible. This is a result of the separation in the time scales of the substrate vibrations and the diffusion of the adsorbed species (e.g. for rhenium atoms on a tungsten surface, the hopping rate is of the order 10^{-2}Hz at room temperature [35] and the Debye frequency of tungsten is of the order 10^{13}Hz). When memory effects are not important, we can make use of the Markov approximation, in which the random forces are completely uncorrelated,

$\langle\vec{\xi}(t)\vec{\xi}(t')\rangle \sim \delta(t-t')$. As mentioned above, this eliminates the memory terms in favor of simple friction terms, giving a standard Langevin equation for the motion of the molecule. In the remainder of this chapter we will derive simplified expressions for the friction tensor and effective potential in the Markov limit.

2.3 Friction Tensor

Notice that the friction tensor is a sum of a contribution from the substrate vibrations, and one from the internal molecular vibrations. Each of the four friction terms $\boldsymbol{B}_{ab}$ have the form

$$\boldsymbol{B}_{ab} = \boldsymbol{B}_{ab}^{(\mathrm{sub})} + \boldsymbol{B}_{ab}^{(\mathrm{int})}, \tag{2.55}$$

where

$$\boldsymbol{B}_{ab}^{(\mathrm{sub})} = \sum_k \frac{\cos[\omega_k(t-t')]}{\omega_k^2} \nabla_a \phi_k^*(X(t)) \nabla_b \phi_k(X(t')), \tag{2.56}$$

$$\boldsymbol{B}_{ab}^{(\mathrm{int})} = \sum_l \frac{\cos[\Omega_l(t-t')]}{\Omega_l^2} \nabla_a \Theta_l(X(t)) \nabla_b \Theta_l(X(t')). \tag{2.57}$$

In this section we will evaluate the substrate friction $\boldsymbol{B}_{ab}^{(\mathrm{sub})}$ by making use of the Debye model for the phonons. The internal friction $\boldsymbol{B}_{ab}^{(\mathrm{int})}$ depends on the vibrational frequencies Ω_l of the molecule being studied. In the simplest approach the normal mode frequencies can be calculated for the isolated molecule. However, some molecules undergo a significant conformational adaptation upon adsorption [36–39]. For such molecules the normal modes can be calculated with the molecule fixed at an adsorption site on the solid; i.e. define the modified internal potential $V_M'(\{\vec{s}_n\}) = V_M(\{\vec{s}_n\}) + V_{MS}(X_{ad}, \{\vec{s}_n\})$, whereX_{ad} stands for the center of mass and angle coordinates at the adsorption site, and calculate the modified normal modes.

2.3.1 Markov Limit

The first simplification we make is to consider the Markov limit, where the memory effects are negligible. We begin by rewriting the memory integral terms in (2.48) and (2.49). Consider the contribution from one of the normal modes in the substrate

friction term $\boldsymbol{B}_{rr}^{(\mathrm{sub})}$ in Eq. (2.48). Taking the t'-independent part outside of the integral, we have

$$\int_0^t \frac{\cos[\omega_k(t-t')]}{\omega_k^2}\nabla_r\phi_k(X(t'))\cdot\dot{\vec{r}}(t')dt' = \int_0^{2\pi/\omega_k} \frac{\cos[\omega_k(t-t')]}{\omega_k^2}\nabla_r\phi_k(X(t'))\cdot\dot{\vec{r}}(t')dt'$$
$$+ \int_{2\pi/\omega_k}^{4\pi/\omega_k} \frac{\cos[\omega_k(t-t')]}{\omega_k^2}\nabla_r\phi_k(X(t'))\cdot\dot{\vec{r}}(t')dt' + \ldots$$
$$+ \int_{2n\pi/\omega_k}^{t} \frac{\cos[\omega_k(t-t')]}{\omega_k^2}\nabla_r\phi_k(X(t'))\cdot\dot{\vec{r}}(t')dt'. \tag{2.58}$$

If the vibration frequency ω_k is fast compared to the time scale for the motion of the adsorbate, the terms that depend on $X(t')$ in the integrals will be approximately constant over the interval $2\pi/\omega_k$. Then all terms except for the last one vanish, and we have

$$\int_0^t \frac{\cos[\omega_k(t-t')]}{\omega_k^2}\nabla_r\phi_k(X(t'))\cdot\dot{\vec{r}}(t')dt' \approx \frac{\sin(\omega_k t)}{\omega_k^3}\nabla_r\phi_k(X(t))\cdot\dot{\vec{r}}(t). \tag{2.59}$$

Using the same procedure on the internal friction term, we recover a set of standard Langevin equations

$$M\ddot{\vec{r}} + \boldsymbol{\beta}_{rr}\cdot\dot{\vec{r}} + \boldsymbol{\beta}_{r\psi}\cdot\dot{\vec{\psi}} + \nabla_r U_{\mathrm{eff}} = \vec{\xi}_r, \tag{2.60}$$
$$\boldsymbol{U}\ddot{\vec{\psi}} + \sum_{jk}\vec{\gamma}_{jk}\dot{\psi}_j\dot{\psi}_k + \boldsymbol{\beta}_{\psi r}\cdot\dot{\vec{r}} + \boldsymbol{\beta}_{\psi\psi}\cdot\dot{\vec{\psi}} + \nabla_\psi U_{\mathrm{eff}} = \vec{\xi}_r, \tag{2.61}$$

where

$$\boldsymbol{\beta}_{ab}(X,t) = \sum_k \frac{\sin(\omega_k t)}{\omega_k^3}\nabla_a\phi_k^*(X)\nabla_b\phi_k(X)$$
$$+ \sum_l \frac{\sin(\Omega_l t)}{\Omega_l^3}\nabla_a\Theta_l(X)\nabla_b\Theta_l(X), \tag{2.62}$$

and the random forces satisfy

$$\langle\vec{\xi}_a(X(t),t)\rangle = 0,$$
$$\langle\vec{\xi}_a(X(t),t)\vec{\xi}_b(X(t'),t')\rangle = 2k_BT\boldsymbol{\beta}_{ab}\delta(t-t'). \tag{2.63}$$

So far we have not made any assumption about the vibrational frequency spectrum of the molecule or solid, or the interaction potential V_{MS}. The Markov approximation,

represented by Eqs. (2.60),(2.62) and (2.63), only requires that the vibrational motion of the molecule and substrate is fast compared to the time scale for the center of mass motion of the molecule. In order to further simplify the substrate friction term, we will now use the Debye model for the substrate vibrations.

2.3.2 Debye Model

We will make use of a bulk Debye model for the solid vibrations, as often employed in surface diffusion and adsorption studies [9, 13, 40–42]. The bulk Debye model is only strictly valid in the interior of an infinite solid, and does not account for surface modes, which modify the phonon frequency spectrum. However, the total contribution to the friction tensor from the phonon interactions involves an integral over the frequency spectrum, and previous work has shown that the difference between a bulk or surface Debye model is negligible [29].

In the bulk Debye model, the normal coordinates $q_{p\vec{k}}$ represent plane waves with wave vector $\vec{k}$ [13],

$$\begin{aligned} q_{p\vec{k}} &= \sqrt{\frac{m_s}{N}}\hat{q}_{p\vec{k}} \cdot \sum_i \vec{u}_i e^{-i\vec{k}\cdot\vec{R}_i^{(0)}}, \\ \vec{u}_i &= \frac{1}{\sqrt{m_s N}} \sum_{p,\vec{k}} q_{p\vec{k}}\hat{q}_{p\vec{k}} e^{i\vec{k}\cdot\vec{R}_i^{(0)}}, \end{aligned} \tag{2.64}$$

where $\hat{q}_{p\vec{k}}$ is the polarization vector for the plane wave represented by $q_{p\vec{k}}$, and N is the number of atoms in the substrate. For each wave vector $\vec{k}$, there will be three normal mode vibrations: one longitudinal and two transverse waves. The frequencies are related to the wave vectors by $\omega_{\vec{k}} = v_s|\vec{k}|$, where v_s is the speed of sound. The coupling constants $\phi_{p\vec{k}}$ then become

$$\phi_{p\vec{k}} = \left(\frac{\partial V_{MS}}{\partial q_{p\vec{k}}}\right)^{(0)} = \sum_i \vec{g}_u^{(i)} \cdot \frac{\partial \vec{u}_i}{\partial q_{p\vec{k}}} = \frac{1}{\sqrt{m_s N}}\hat{q}_{p\vec{k}} \cdot \sum_i \vec{g}_u^{(i)} e^{i\vec{k}\cdot\vec{R}_i^{(0)}}, \tag{2.65}$$

and the substrate friction tensor is

$$\begin{aligned} \boldsymbol{\beta}_{ab}^{(\mathrm{sub})} &= \sum_{i,j} \nabla_a \vec{g}_u^{(i)} \cdot \frac{1}{N} \sum_{p,\vec{k}} \frac{\sin(\omega_{\vec{k}} t)}{m_s \omega_{\vec{k}}^3} e^{i\vec{k}\cdot(\vec{R}_i^{(0)} - \vec{R}_j^{(0)})} \hat{q}_{p\vec{k}} \hat{q}_{p\vec{k}}^* \cdot \nabla_b \vec{g}_u^{(j)} \\ &= \sum_{i,j} \nabla_a \vec{g}_u^{(i)} \cdot \nabla_b \vec{g}_u^{(j)} \frac{1}{N} \sum_{\vec{k}} \frac{\sin(\omega_{\vec{k}} t)}{m_s \omega_{\vec{k}}^3} e^{i\vec{k}\cdot(\vec{R}_i^{(0)} - \vec{R}_j^{(0)})}, \end{aligned} \tag{2.66}$$

where the second line follows because the three polarization vectors for a given $\vec{k}$ are mutually orthogonal, so $\sum_p \hat{q}_{p\vec{k}}\hat{q}^*_{p\vec{k}} = \mathbf{1}$, where $\mathbf{1}$ is the identity matrix. The allowed values for the wave vector are $\vec{k} = \frac{\pi}{L}(n_x\hat{x} + n_y\hat{y} + n_z\hat{z})$, where n_x, n_y and n_z are integers, and L is the macroscopic length of the solid. Approximating the sum over $\vec{k}$ by an integral, the integration will go over a sphere in $\vec{k}$ space with a radius k_D chosen so that $\frac{4}{3}\pi k_D^3/(\frac{\pi}{L})^3 = N$, giving the correct number of normal modes. Eq. (2.66) then becomes

$$\begin{aligned}\boldsymbol{\beta}^{(\mathrm{sub})}_{ab} = &\sum_{i,j} \nabla_a \vec{g}^{(i)}_u \cdot \nabla_b \vec{g}^{(j)}_u \frac{1}{N}\left(\frac{L}{\pi}\right)^3 \\ &\times \int_0^{k_D} \frac{\sin(\omega_{\vec{k}} t)}{m_s \omega^3_{\vec{k}}} k^2 dk \int_0^{2\pi} d\phi \int_0^{\pi} d\theta \sin(\theta) e^{ikR_{ij}\cos(\theta)},\end{aligned} \tag{2.67}$$

where $R_{ij} = |\vec{R}^{(0)}_i - \vec{R}^{(0)}_j|$. Performing the angular integral and rewriting the integral over k as an integral over ω gives

$$\boldsymbol{\beta}^{(\mathrm{sub})}_{ab} = \sum_{i,j} \nabla_a \vec{g}^{(i)}_u \cdot \nabla_b \vec{g}^{(j)}_u \frac{3}{m_s \omega_D^3} \int_0^{\omega_D} \frac{\sin(\omega t)}{\omega} \frac{\sin(\omega R_{ij}/v_s)}{\omega R_{ij}/v_s} d\omega, \tag{2.68}$$

where $\omega_D = v_s k_D$ is the Debye frequency. Rewriting the integral over ω using $u = \omega t$ gives

$$\int_0^{\omega_D t} \frac{\sin(u)}{u} \frac{\sin(uR_{ij}/(v_s t))}{uR_{ij}/(v_s t)} du. \tag{2.69}$$

Assuming the interaction potential V_{MS} is short ranged, only substrate atoms within some finite radius of the adsorbed molecule will interact with it, so we need only consider pairs of substrate atoms within such a radius in the substrate friction, Eq. (2.68). Then $R_{ij}/(v_s t)$, which is the ratio of the time for a sound wave to travel between substrate atoms i and j to the macroscopic time t for the motion of the molecule, will be vanishingly small, in which case the second factor in the integral tends to 1. Also, since $\omega_D t \gg 1$, we can take the upper integration limit to be ∞, and the integral has the value $\pi/2$. The substrate friction now takes the form

$$\boldsymbol{\beta}^{(\mathrm{sub})}_{ab} = \frac{3\pi}{2m_s\omega_D^3} \sum_i \nabla_a \vec{g}^{(i)}_u \cdot \sum_j \nabla_b \vec{g}^{(j)}_u. \tag{2.70}$$

The final simplification comes from assuming the interaction potential V_{MS} consists of a sum of pairwise interactions,

$$V_{MS} = \sum_{i,j} v_{ij}(\vec{R}_i - \vec{r}_j), \tag{2.71}$$

so that

$$\sum_i \vec{g}_u^{(i)} = \sum_i (\nabla_{R_i} V_{MS})^{(0)} = \sum_{i,j} \nabla v_{ij}(\vec{R}_i^{(0)} - \vec{r}_j) = -\sum_{i,j} \nabla_{r_j} v_{ij}(\vec{R}_i^{(0)} - \vec{r}_j) = -\nabla_r V_{MS}^{(0)}, \tag{2.72}$$

where we have used the fact that $\nabla_r = \sum_i \nabla_{r_i}$. Finally, we have the following simple expression for the substrate friction tensor

$$\boldsymbol{\beta}_{ab}^{(\mathrm{sub})}(X) = \frac{3\pi}{2m_s\omega_D^3} \nabla_a \nabla_r V_{MS}^{(0)}(X) \cdot \nabla_b \nabla_r V_{MS}^{(0)}(X). \tag{2.73}$$

2.3.3 Friction For a Dimer in 1D

In this section we derive an expression for the friction tensor for a dimer in one dimension, to be used for calculations in the next chapter. Consider a dimer with center of mass coordinate $r = (m_1 x_1 + m_2 x_2)/M$ and dimer length $s = x_1 - x_2$, where x_1 and x_2 are the positions of the two atoms of the dimer along the surface. Since the dimer is confined to 1D, its angle coordinates are fixed, so we need only to consider the center of mass equation. In 1D it reads

$$M\ddot{r} + \beta_{rr}\dot{r} + \frac{\partial U_{\mathrm{eff}}}{\partial r} = \xi_r. \tag{2.74}$$

If the interaction potential for each atom with the solid is $V(x)$, the total interaction potential will be

$$V_{MS}(r, s) = V(r + \tfrac{m_2}{M}s) + V(r - \tfrac{m_1}{M}s), \tag{2.75}$$

and the substrate friction, Eq. (2.73), is

$$\beta_{rr}^{(\mathrm{sub})}(r) = \frac{3\pi}{2m_s\omega_D^3} \left[\frac{\partial^2 V_{MS}}{\partial r^2}\right]^2 \Bigg|_{s=s_0}, \tag{2.76}$$

where s_0 is the equilibrium dimer length.

In the harmonic approximation, the internal potential is

$$V_M(s) = \frac{1}{2}\mu\Omega^2(s - s_0)^2, \tag{2.77}$$

where $\mu = (1/m_1 + 1/m_2)^{-1}$ is the reduced mass of the dimer. The normal coordinate for the internal vibration of the dimer is $\alpha = \sqrt{\mu}(s - s_0)$, and the coupling constant Θ is therefore

$$\Theta = \left.\frac{\partial V_{MS}}{\partial \alpha}\right|_{\alpha=0} = \frac{1}{\sqrt{\mu}} \left.\frac{\partial V_{MS}}{\partial s}\right|_{s=s_0} \tag{2.78}$$

The internal friction is then given, in the Markov limit, by Eq. (2.62)

$$\beta_{rr}^{(\mathrm{int})}(r,t) = \frac{\sin(\Omega t)}{\mu\Omega^3} \left.\left[\frac{\partial^2 V_{MS}}{\partial r \partial s}\right]^2\right|_{s=s_0}. \tag{2.79}$$

For simplicity, in the next chapter we will consider the stiff dimer limit, $\Omega \gg \omega_D$, so that $B_{rr}^{(\mathrm{int})}$ is negligible compared to $B_{rr}^{(\mathrm{sub})}$.

With Eq. (2.76), the position dependant friction coefficient is given once the interaction potential V_{MS} is specified. In the next chapter we will consider a simple model potential, and perform a calculation of the diffusion coefficient.

2.4 Effective Potential

The effective potential, Eq.(2.53), has the form

$$U_{\mathrm{eff}} = V_{MS}^{(0)} + U_{\mathrm{eff}}^{(\mathrm{sub})} + U_{\mathrm{eff}}^{(\mathrm{int})}. \tag{2.80}$$

In this section we derive a simplified expression for $U_{\mathrm{eff}}^{(\mathrm{sub})}$ by making use of the Debye model for the substrate vibrations, and an expression for $U_{\mathrm{eff}}^{(\mathrm{int})}$ for a dimer in 1D.

2.4.1 Debye Model

Making use of Eq. (2.65) for the coupling constants ϕ_k in the Debye model, the contribution to the effective potential from the substrate vibrations is

$$\begin{aligned} U_{\mathrm{eff}}^{(\mathrm{sub})} &= -\frac{1}{2}\sum_{j,\vec{k}} \frac{|\phi_{j,\vec{k}}|^2}{\omega_{j,\vec{k}}^2} \\ &= \frac{1}{m_s N}\left(\frac{L}{\pi}\right)^3 \sum_{i,j} \vec{g}_u^{(i)} \cdot \vec{g}_u^{(j)} \int_0^{k_D} \frac{k^2}{\omega_k^2} dk \int_0^{2\pi} d\phi \int_0^{\pi} d\theta \sin\theta e^{ikR_{ij}\cos\theta}, \end{aligned} \tag{2.81}$$

where $R_{ij} = |\vec{R}_i - \vec{R}_j|$. Evaluating the angular integrals and rewriting the integral over k as an integral over ω gives

$$U_{\text{eff}}^{(\text{sub})} = -\frac{3}{2m_s\omega_D^3}\sum_{i,j}\vec{g}_u^{(i)}\cdot\vec{g}_u^{(j)}\frac{v_s}{R_{ij}}\int_0^{\frac{\omega_D R_{ij}}{v_s}}\frac{\sin u}{u}. \tag{2.82}$$

Again, we only need to consider pairs of substrate atoms i and j in the vicinity of the molecule, in which case $\frac{\omega_D R_{ij}}{v_s} \lesssim 1$, and we have

$$\begin{aligned} U_{\text{eff}}^{(\text{sub})} &\approx -\frac{3}{2m_s\omega_D^3}\sum_{i,j}\vec{g}_u^{(i)}\cdot\vec{g}_u^{(j)}\frac{v_s}{R_{ij}}\frac{\omega_D R_{ij}}{v_s} \\ &= -\frac{3}{2m_s\omega_D^2}\nabla_r V_{MS}^{(0)}\cdot\nabla_r V_{MS}^{(0)}. \end{aligned} \tag{2.83}$$

The effective potential appears in the center of mass equations as

$$\nabla_r U_{\text{eff}}^{(\text{sub})} = \frac{-3}{m_s\omega_D^2}\nabla_r\nabla_r V_{MS}^{(0)}\cdot\nabla_r V_{MS}^{(0)}. \tag{2.84}$$

Since the interactions are short ranged, $\nabla_r\nabla_r V_{MS}^{(0)}$ is of the same order of magnitude as $\nabla_{R_i}\nabla_{R_j}V_{MS}^{(0)}$. Also, $m_s\omega_D^2$ is the largest value of the matrix $\nabla_{R_i}\nabla_{R_j}V_S^{(0)}$. Since, by assumption, $\nabla_{R_i}\nabla_{R_j}V_{MS}^{(0)} \ll \nabla_{R_i}\nabla_{R_j}V_S^{(0)}$, the effective potential term $\nabla_r U_{\text{eff}}^{(\text{sub})}$ will be negligible compared to $\nabla_r V_{MS}^{(0)}$.

2.4.2 Effective Potential For a Dimer in 1D

For a dimer in 1D, the contribution to the effective potential from the internal vibrations of the dimer is

$$U_{\text{eff}}^{(\text{int})} = -\frac{1}{2}\frac{\Theta^2}{\Omega^2} = -\frac{1}{2\mu\Omega^2}\left(\frac{\partial V_{MS}}{\partial s}\right)^2\Bigg|_{s=s_0}. \tag{2.85}$$

A similar argument to that used for $U_{\text{eff}}^{(\text{sub})}$ can be used to show that $U_{\text{eff}}^{(\text{int})}$ is negligible compared to the interaction potential V_{MS}. The effective potential appears in the center of mass equation (in 1D) as

$$\frac{\partial U_{\text{eff}}^{(\text{int})}}{\partial r} = -\frac{1}{\mu\Omega^2}\frac{\partial^2 V_{MS}}{\partial r\partial s}\frac{\partial V_{MS}}{\partial s}. \tag{2.86}$$

The first factor $\frac{\partial^2 V_{MS}^{(0)}}{\partial r\partial s}$ is of the same order of magnitude as $\frac{\partial^2 V_{MS}^{(0)}}{\partial r^2} \sim \nabla_{R_i}\nabla_{R_j}V_{MS}^{(0)}$, and $\mu\Omega^2 = \frac{\partial^2 V_{MS}^{(0)}}{\partial s^2}$. Since, by assumption, $\nabla_{R_i}\nabla_{R_j}V_{MS}^{(0)} \ll \frac{\partial^2 V_{MS}^{(0)}}{\partial s^2}$, the effective potential

term $\frac{\partial U_{\text{eff}}^{(\text{int})}}{\partial r}$ will be negligible compared to $\frac{\partial V_{MS}^{(0)}}{\partial r}$. In the calculations that follow, we will therefore ignore $U_{\text{eff}}^{(\text{sub})}$ and $U_{\text{eff}}^{(\text{int})}$, and set $U_{\text{eff}} = V_{MS}^{(0)}$.

Chapter 3

Dimer Diffusion

In this chapter we will consider diffusion in one dimension, with the adatom-surface interaction given by the following model potential

$$V(x) = V_a \exp\left[a\cos\left(\frac{2\pi}{l}x\right)\right] - \bar{V}, \tag{3.1}$$

where $V_a = V_0/(e^a - e^{-a})$, and $\bar{V} = \frac{V_0}{2}(e^a + e^{-a})/(e^a - e^{-a})$. The energy barrier (i.e. the difference between the minimum and maximum values of $V(x)$) is V_0. The shape of this potential depends on the parameter a. When a is small, the potential approaches a cosine, i.e. for $a \to 0$ we have $V(x) \to \frac{V_0}{2}\cos\left(\frac{2\pi}{l}x\right)$. As a is increased, the bottom of the potential well becomes more broad and flat. Some plots of this potential for a few values of a are given in Fig. 3.1.

We will calculate the diffusion coefficient D for one dimensional motion in this potential. The equation of motion for 1D diffusion is

$$m\ddot{r} + \beta(r)\dot{r} + \frac{\partial V_{MS}}{\partial r} = \xi. \tag{3.2}$$

We consider the high friction, or Smoluchowski limit, in which the inertial term $m\ddot{r}$ is negligible compared to the friction, giving

$$\beta(r)\dot{r} + \frac{\partial V_{MS}}{\partial r} = \xi. \tag{3.3}$$

In this limit we can calculate D by making use of the high friction result given in Chapter 1,

$$D = k_B T\left[\frac{1}{l}\int_0^l \beta(x)e^{V_{MS}(x)/k_BT}dx\frac{1}{l}\int_0^l e^{-V_{MS}(x')/k_BT}dx'\right]^{-1}. \tag{3.4}$$

In the remainder of this chapter we will first consider diffusion of a single atom, and then move on to treat dimer diffusion.

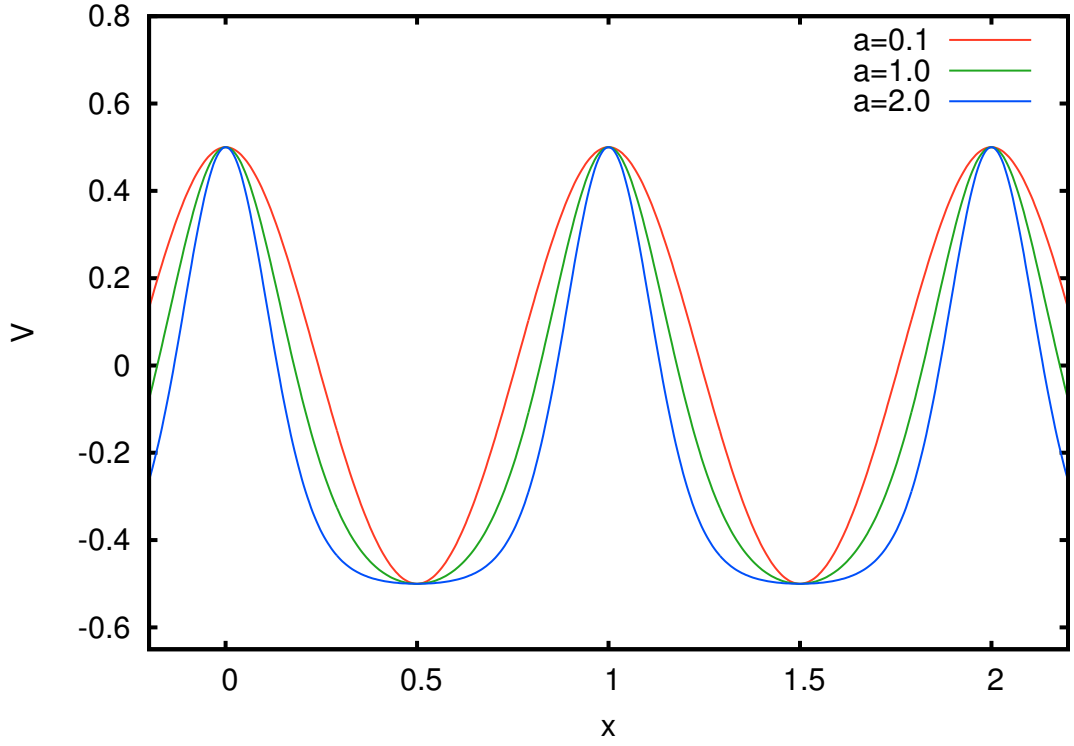

Figure 3.1: The adatom-surface interaction potential, shown for a few values of the parameter a. It can be seen that as a gets larger the potential becomes more flattened at the minimum. Length is shown in units of l, and potential in units of V_0. (The same convention is used for all plots in this thesis.)

3.1 Single Atom

Consider a single atom in 1D with coordinate x. For the interaction potential V_{MS} given by Eq. (3.1), the friction coefficient is found from Eq. (2.76),

$$\begin{aligned}\beta(x) &= \frac{3\pi}{2m_s\omega_D^3}[V''(x)]^2 \\ &= \frac{3\pi}{2m_s\omega_D^3}\left(\frac{2\pi}{l}\right)^4 V_a^2\left[a^2\sin\left(\frac{2\pi}{l}x\right) - a\cos\left(\frac{2\pi}{l}x\right)\right]^2 e^{2a\cos\left(\frac{2\pi}{l}x\right)}\end{aligned} \tag{3.5}$$

We can obtain analytical results for the single atom in two special cases. First, in the limit $a \to 0$, when the potential approaches a simple cosine, the result has been previously found to be [9]

$$D = \frac{\bar{D}}{12\pi^5}\frac{1}{I_0(\gamma)[\gamma I_0(\gamma) - I_1(\gamma)]}, \tag{3.6}$$

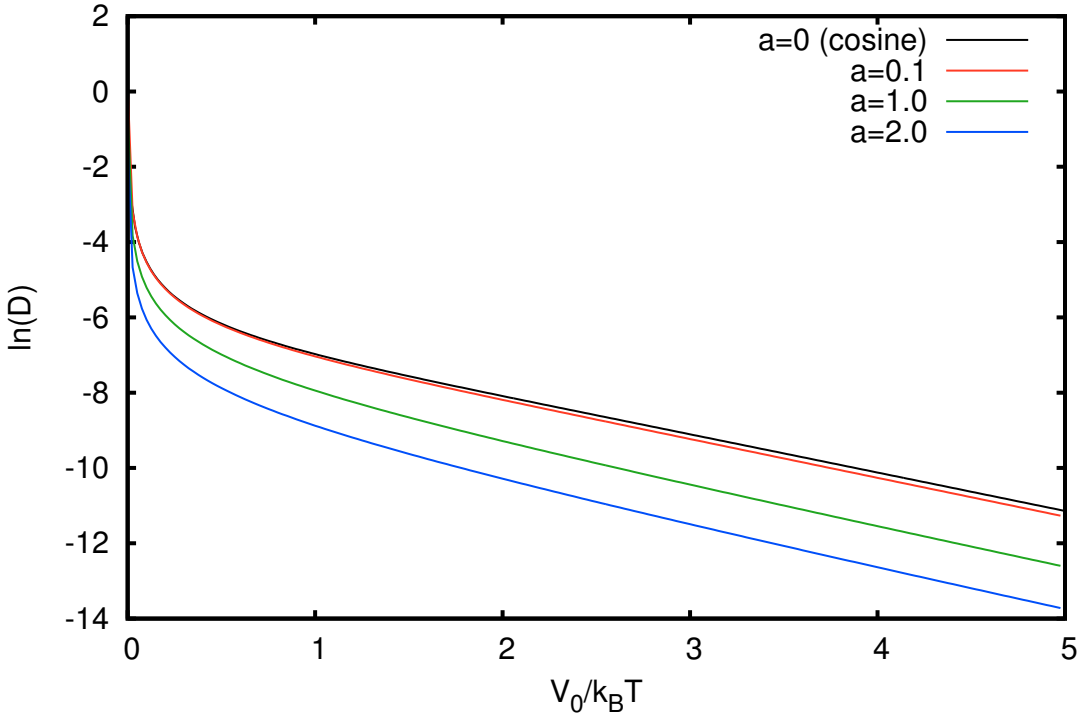

Figure 3.2: $\ln(D)$ vs V_0/k_BT for a single atom. The deviation from the Arrhenius form can be seen for small barriers. In the plot, D has been scaled by the constant $\bar{D}$; the same convention is used for all plots in this thesis.

where $\bar{D} = \frac{m_s\omega_D^3 l^4}{V_0}$, and $\gamma = \frac{V_0}{2k_BT}$. The functions I_0 and I_1 are modified Bessel functions of the first kind. In the limit $\gamma \gg 1$, corresponding to high barriers, the Bessel functions asymptotically tend to $e^\gamma/\sqrt{2\pi\gamma}$ [43], and Eq. (3.6) becomes

$$D = \frac{\bar{D}}{6\pi^4} e^{-V_0/k_BT}. \tag{3.7}$$

So for high diffusion barriers D has the Arrhenius form $D = D_0 e^{-\Delta V/k_BT}$, which is expected. For low barriers, D deviates from the Arrhenius form as seen in figure 3.2, which shows plots of $\ln(D)$ vs V_0/k_BT. The deviation from a straight line can be clearly seen at small γ.

We can also obtain an analytical result for $a > 0$ in the limit of large barriers, $\gamma \gg 1$. In this limit, because of the exponential term, only the region around the maximum of V_{MS} will contribute significantly to the first integral in (3.4). We can

therefore expand V_{MS} around the maximum at $x = 0$ to get

$$V_{MS}(x) \approx V_a e^a - \bar{V} - \frac{1}{2} V_a \left(\frac{2\pi}{l}\right)^2 a e^a x^2. \tag{3.8}$$

To a first approximation, we can also replace the position dependant friction $\beta(x)$ with its value at this maximum,

$$\beta(x) \approx \frac{3\pi}{2 m_s \omega_D^3} V_a^2 \left(\frac{2\pi}{l}\right)^4 a^2 e^{2a}. \tag{3.9}$$

Similarly, the largest contribution to the second integral will be from the region around the minimum at $x = l/2$, so we can expand V_{MS} around the minimum to get

$$V_{MS}(x) \approx V_a e^{-a} - \bar{V} + \frac{1}{2} V_a \left(\frac{2\pi}{l}\right)^2 a e^a (x - l/2)^2. \tag{3.10}$$

Making these substitutions, the integrals can easily be evaluated to give

$$D = \frac{\bar{D}}{12\pi^4} \frac{e^{-a} - e^{-3a}}{a} e^{-V_0/k_B T}. \tag{3.11}$$

So, as expected, the diffusion coefficient has the Arrhenius form in the limit of high barriers. The prefactor depends strongly on the parameter a, which determines the shape of the potential; it decreases exponentially as the minimum of the potential well becomes more broad and flat. This decrease can also be seen in Fig. 3.2. Also note that in the limit $a \to 0$, Eq. (3.11) reduces to the correct result for a cosine potential, Eq. (3.7).

3.2 Dimer

For a dimer of two identical atoms at positions x_1 and x_2, the interaction potential will be

$$V_{MS}(x_1, x_2) = V(x_1) + V(x_2) = V(r + s/2) + V(r - s/2) \tag{3.12}$$

where $V(x)$ is given by Eq. (3.1), and r and s are the center of mass and dimer length.

Again, we begin with the cosine potential, corresponding to $a \to 0$, for which we can obtain some simple analytical results for the diffusion coefficient. In this case the surface potential can be written

$$V_{MS}(r, s) = V_0 \cos\left(\frac{\pi}{l} s\right) \cos\left(\frac{2\pi}{l} r\right). \tag{3.13}$$

The energy barrier for this potential depends on the dimer length, and is given by $\Delta V = 2V_0|\cos\left(\frac{\pi}{l}s\right)|$.

The friction coefficient is found from Eq. (2.76),

$$\beta(r) = \frac{3\pi}{2m_s\omega_D^3}\left[\frac{\partial^2 V_{MS}}{\partial r^2}\right]^2\Bigg|_{s=s_0} = \frac{3\pi}{2m_s\omega_D^3}V_0^2\left(\frac{2\pi}{l}\right)^4\cos^2\left(\frac{\pi}{l}s_0\right)\cos^2\left(\frac{2\pi}{l}r\right) \quad (3.14)$$

The integrals in Eq. (3.4) can then be evaluated using standard integration tables [43], and the resulting diffusion coefficient is

$$D_s = \frac{\bar{D}}{24\pi^5\cos\left(\frac{\pi}{l}s_0\right)}\frac{1}{I_0(\gamma)[\gamma I_0(\gamma) - I_1(\gamma)]} \quad (3.15)$$

where $\gamma = V_0\cos\left(\frac{\pi}{l}s_0\right)/k_BT$. For large barriers, that is $|\gamma| \gg 1$, this becomes

$$D_s = \frac{\bar{D}}{12\pi^4|\cos\left(\frac{\pi}{l}s_0\right)|}e^{-2V_0|\cos\left(\frac{\pi}{l}s_0\right)|/k_BT}. \quad (3.16)$$

So again, in the limit of large barriers, the diffusion coefficient has the Arrhenius form.

Note that when the dimer length s_0 goes to 0, this reduces to

$$D = \frac{m_s\omega_D^3 l^4}{6\pi^4(2V_0)}e^{-(2V_0)/k_BT}, \quad (3.17)$$

which is the correct result for a single atom in a cosine potential with a barrier of $2V_0$ (compare with Eq. (3.7)).

A similar calculation was performed by Ruckenstein and Tsekov [9], but using a constant friction coefficient

$$\beta = \frac{12\pi}{m_s\omega_D^3}\frac{V_0^2\pi^4}{l^4} \quad (3.18)$$

instead of the position dependant friction $\beta(r)$. They also neglect the off-diagonal terms ($i \neq j$) in the memory-friction tensor $\boldsymbol{B}_{ij}$, Eq. (2.17), assuming the fluctuation-dissipation processes in the two atoms of the dimer to be independent. Their result for the diffusion coefficient, in the limit of large barriers, is

$$D = \bar{D}\frac{|\cos\left(\frac{\pi}{l}s_0\right)|}{6\pi^4}e^{-2V_0|\cos\left(\frac{\pi}{l}s_0\right)|/k_BT} \quad (3.19)$$

The reason for the difference between the results of Eqs. (3.16) and (3.19) is the following. As mentioned in the previous section, at high barriers the friction coefficient can be replaced by its value at the potential maximum, and indeed it can be verified that replacing $\beta(r)$ as defined in Eq. (3.14) with the constant

$$\begin{aligned}\beta(r_{\max}) &= \frac{3\pi}{2m_s\omega_D^3}V_0^2\left(\frac{2\pi}{l}\right)^4\cos^2\left(\frac{\pi}{l}s_0\right)\cos^2\left(\frac{2\pi}{l}\frac{nl}{2}\right)\\ &= \frac{3\pi}{2m_s\omega_D^3}V_0^2\left(\frac{2\pi}{l}\right)^4\cos^2\left(\frac{\pi}{l}s_0\right)\end{aligned} \tag{3.20}$$

yields the same result for D, Eq. (3.16). (We have used the fact that the maximum of the potential (3.12) occurs at $r_{\max} = nl/2$, where n is an odd integer when $0 < s_0 < l/2$ and an even integer when $l/2 < s_0 < l$.) Now notice that the value used by Ruckenstein and Tsekov for the friction coefficient is simply twice the friction coefficient of a single atom in the cosine potential. That is, they use

$$\beta = \frac{3\pi}{2m_s\omega_D^3}[V''(0)^2 + V''(0)^2] = \frac{3\pi}{2m_s\omega_D^3}\frac{V_0^2}{2}\left(\frac{2\pi}{l}\right)^4, \tag{3.21}$$

so their result is different from Eq. (3.16) by a factor of $2\cos^2\left(\frac{\pi}{l}s_0\right)$.

A plot comparing our result for the diffusion prefactor (defined in Eq. (3.16)) with that of Ruckenstein and Tsekov (defined in Eq. (3.19)) is given in figure 3.3. Note that at as $s_0 \to l/2$, neither result is valid, since in that case the potential becomes flat, $V_{MS}^{(0)} = V_0\cos(\frac{\pi}{l}s_0)\cos(\frac{2\pi}{l}r) = 0$, and so both the barrier $\Delta V = 2V_0|\cos\left(\frac{\pi}{l}s\right)|$ and the friction coefficient goes to 0. This means that neither the high barrier approximation or the high friction approximation are valid. The results clearly show different qualitative behavior of the prefactor as a function of the dimer length. Our result (3.16) increases as s_0 increases from 0 to $l/2$, while Ruckenstein and Tsekov's result (3.19) decreases. The difference in the results is due to the inclusion of the off diagonal friction terms and position dependence of the friction in our calculation. Even when we take the limit of high barriers, so that the position dependent friction is replaced with the spatially constant friction $\beta = \beta(r_{\max})$, β still depends on the dimer length s_0, so the behavior as a function of s_0 is different from the case of a constant friction coefficient as used in Ref. [9]. Several other studies of dimer diffusion have also made use of a constant friction coefficient [8, 22, 44, 45]. However, the

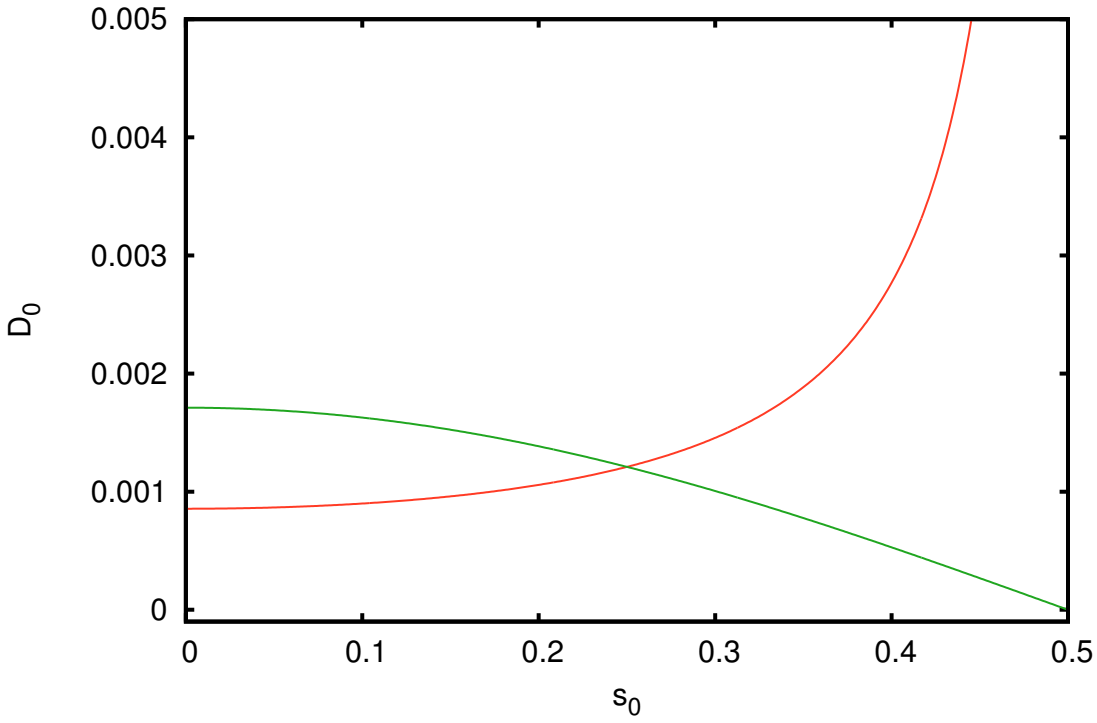

Figure 3.3: A comparison of our result for the diffusion prefactor (3.16) (red line) for a cosine potential with Ruckenstein and Tsekov's result (3.19) (green line).

results here suggest that including the dependence of the friction coefficient on the dimer length has a significant effect on the diffusion prefactor.

To find the diffusion coefficient when $a > 0$, the integrals in Eq. (3.4) must be performed numerically. A plot of D for a few values of a and s_0 is shown in figure 3.4. It can be seen that, similar to the single atom diffusion coefficient, D has the Arrhenius form when the diffusion barrier is large, and deviates from this behavior when it is small. The prefactor and energy barrier can be obtained for large barriers by doing a fit of $D(T)$ to $D(T) = D_0 e^{-\Delta V/k_B T}$. The barriers and prefactors obtained in this way are shown in Figs. 3.5 and 3.6 as a function of the dimer length, for a few values of the parameter a. Note that the barriers shown in Fig. 3.5 are effective activation barriers and do not necessarily correspond to the difference in potential energy between the minimum and transition state, since the dimer potential can develop local minima at certain dimer lengths (see Fig. 3.7). In these plots the range of the dimer length is $s_0 = 0$ to $s_0 = l$, chosen because letting $s_0 \to s_0 + l$ just

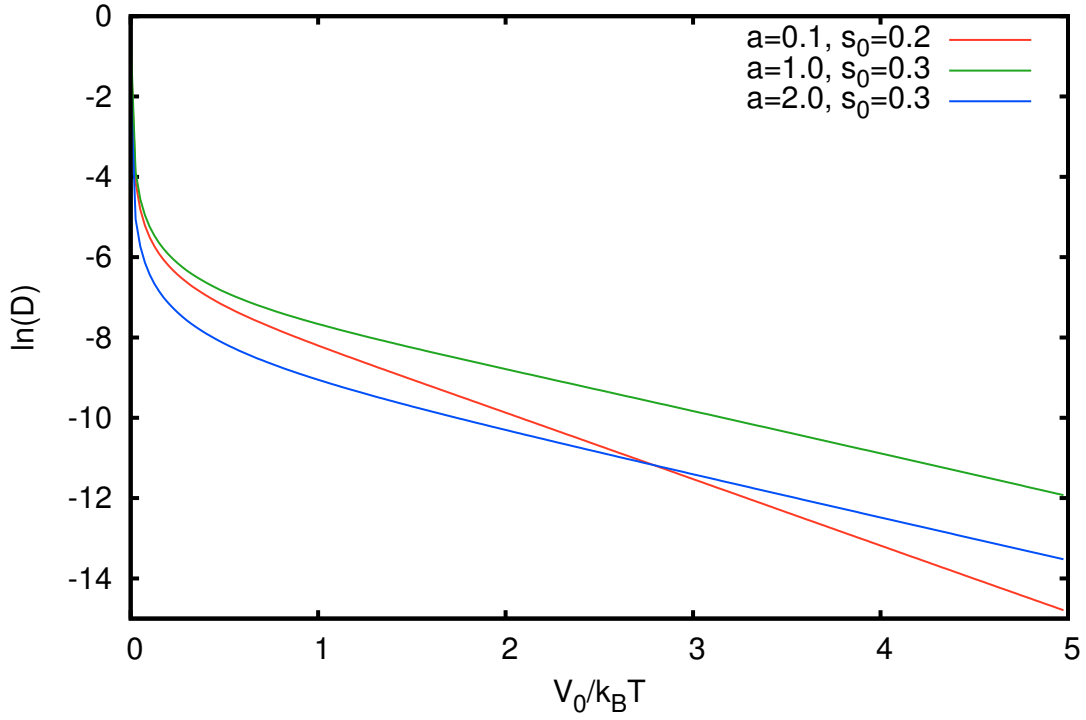

Figure 3.4: The diffusion coefficient D as a function of inverse temperature V_0/k_BT for a dimer.

introduces an offset in r to the potential, which does not affect the results. Letting $s_0 \to l - s_0$ has the same effect, so D should be periodic in s_0 with period l, and even around $s_0 = (n + 1/2)l$ (where n is an integer). This can be seen to be the case in Figs. 3.5 and 3.6.

It can be seen from Fig. 3.5 that the energy barrier ΔV for a dimer can be larger or smaller than that for a single atom, depending on the dimer length s_0. For example, for the case of $a = 0.1$, dimers with equilibrium length between $s_0 \approx 0.34l$ and $s_0 \approx 0.66l$ will have a smaller barrier than a single atom. The dimer length at which ΔV for the dimer crosses the single atom value does not depend strongly on the shape of the potential, occurring at approximately $s_0 \approx 0.3l$ and $s_0 \approx 0.7l$, regardless of the value of the shape parameter a. The barrier has its minimum value at $s_0 = l/2 + nl$, and its maximum value at $s_0 = nl$, where n is an integer. This has a simple interpretation: when the dimer length is a multiple of the lattice constant, both atoms can sit at the bottom of the potential well and the barrier is simply twice

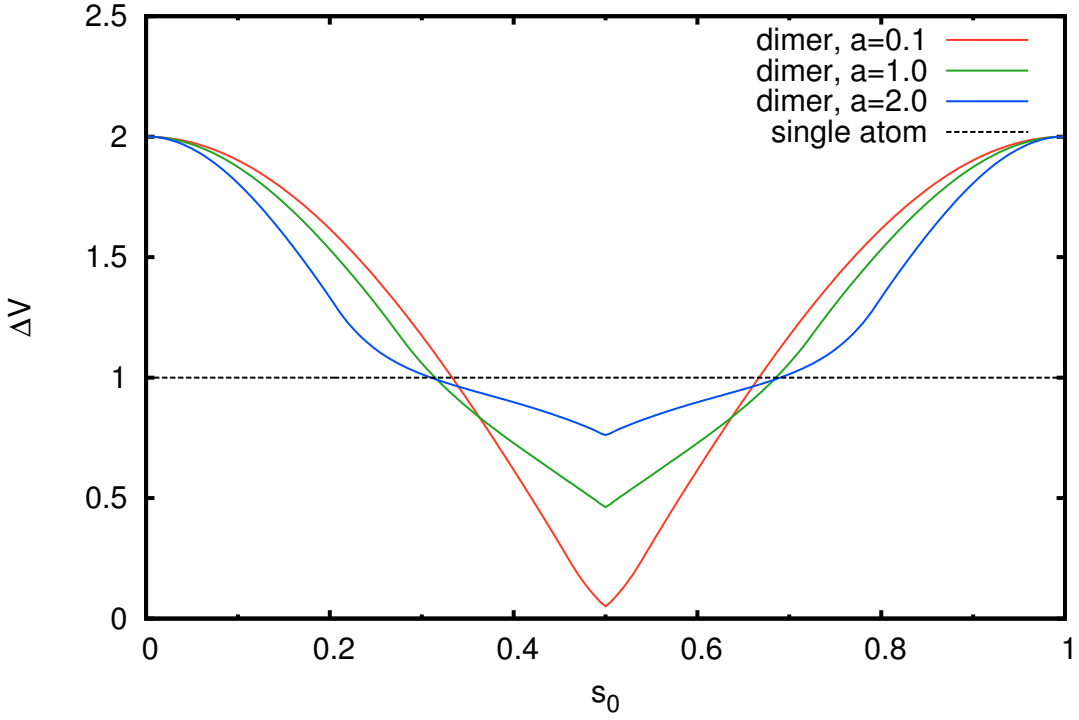

Figure 3.5: The potential energy barrier ΔV as a function of dimer length s_0. The barrier for a single atom is shown for comparison. The temperature range used in the Arrhenius fit was $V_0/k_BT = 100$ to $V_0/k_BT = 105$

that for a single atom. When the dimer length is not commensurate with the lattice spacing, the atoms are forced to sit higher in the potential well than single atoms would, so the effective diffusion barrier is decreased.

The most interesting feature of Fig. 3.6 is that the prefactors exhibit a maximum as a function of the dimer length. The reason for this is as follows. As shown in the previous section, for large barriers the diffusion prefactor is approximately inversely proportional to the friction at the potential maximum, $D_0 \sim 1/\beta(r_{\max})$, so a maximum in D_0 corresponds to a minimum in $\beta(r_{\max})$. The friction is proportional to the second derivative of V_{MS}, so if the curvature of V_{MS} goes to zero at the maximum (i.e. the potential is locally flat), there should be a maximum in D_0. This does in fact happen when a local minimum appears at $r = nl$ as the dimer length s_0 is changed. This is shown in figure 3.7 for the case $a = 1.0$. It can be seen that the local minimum at $r = nl$ appears when $s_0 \gtrsim 0.3l$, which coincides with the maximum

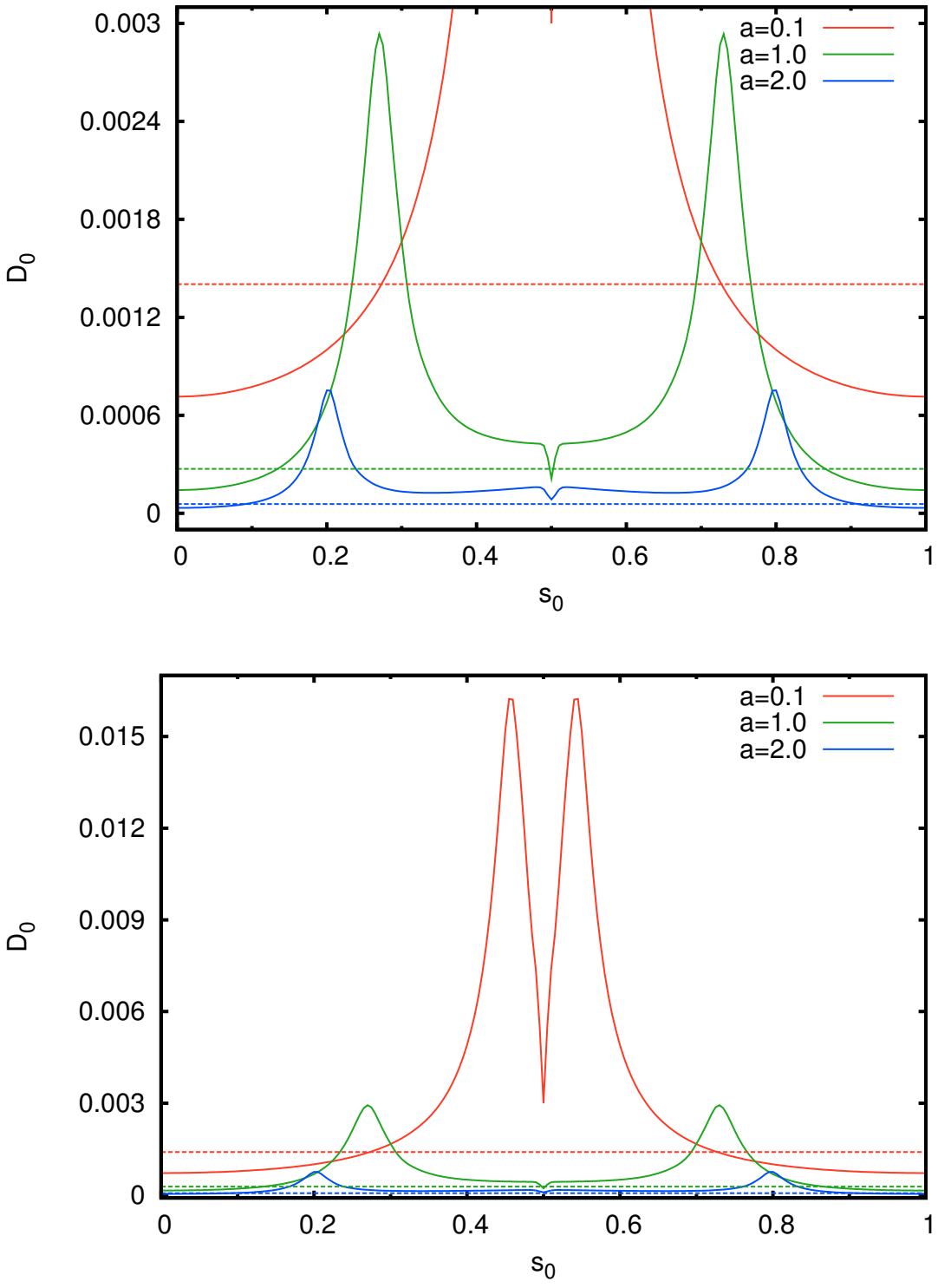

Figure 3.6: The diffusion coefficient prefactor D_0 as a function of dimer length s_0, plotted on two different scales for clarity. The single atom values are shown as dashed lines for comparison. The temperature range used in the Arrhenius fit was $V_0/k_BT = 100$ to $V_0/k_BT = 105$

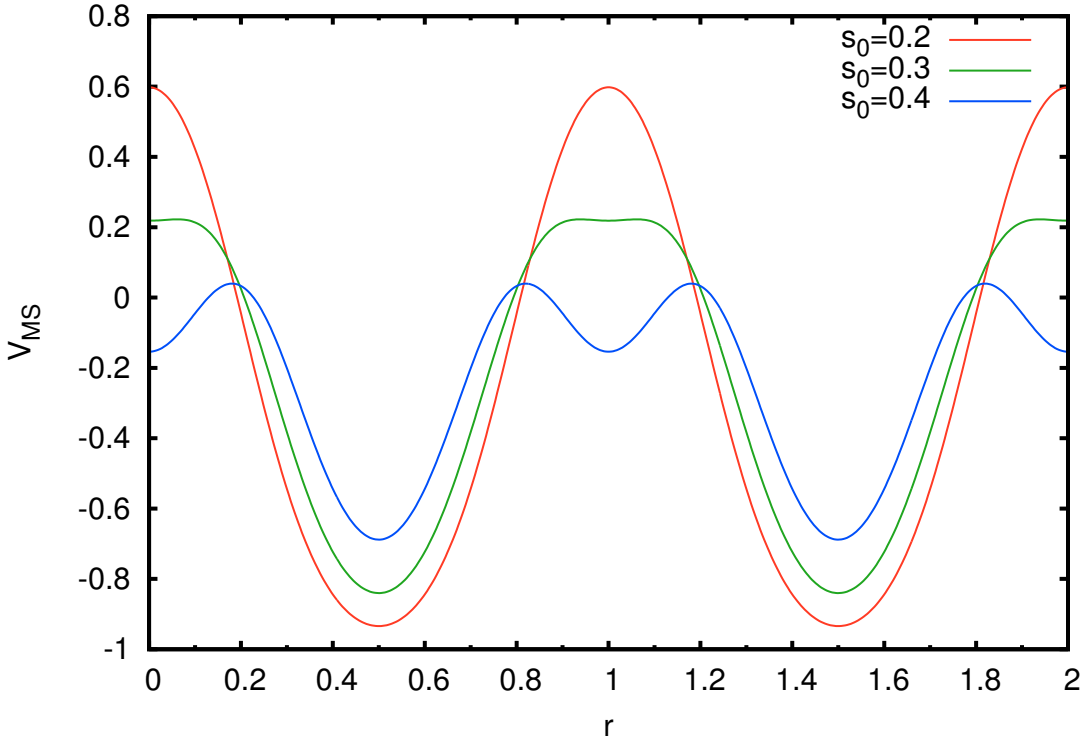

Figure 3.7: The dimer potential $V_{MS}(r)$ with $a = 1.0$ for a few values of the dimer length s_0. It can be seen that the local minimum appears around $s_0 \simeq 0.3l$.

in D_0 seen in Fig. 3.6. The exact value of s_0 for which the local minimum in the dimer potential (and the peak in the dimer prefactor) appears can be found by considering the second derivative of the dimer potential, Eq. (3.12). At $r = 0$ it has the value

$$V''_{MS}(0) = -2aV_a \left(\frac{2\pi}{l}\right)^2 \left[a\cos^2\left(\frac{\pi}{l}s_0\right) + \cos\left(\frac{\pi}{l}s_0\right) - a\right] e^{a\cos\left(\frac{\pi}{l}s_0\right)}. \tag{3.22}$$

Setting $V''_{MS}(0) = 0$ gives

$$a\cos^2\left(\frac{\pi}{l}s_0\right) + \cos\left(\frac{\pi}{l}s_0\right) - a = 0, \tag{3.23}$$

which has the solutions

$$\cos\left(\frac{\pi}{l}s_0\right) = -\frac{1}{2a}\left(1 \pm \sqrt{1+4a^2}\right). \tag{3.24}$$

The solution between $s_0 = 0$ and $s_0 = l/2$ gives

$$\frac{s_0}{l} = \frac{1}{\pi}\cos^{-1}\left(\frac{\sqrt{1+4a^2}-1}{2a}\right). \tag{3.25}$$

For $a = 0.1, 1.0, 2.0$, this gives $s_0/l = 0.47, 0.29, 0.21$, respectively, which agrees with Fig. 3.6. For dimer lengths close to the value at which the maximum in the prefactor occurs, the dimer prefactor is larger than prefactor for a single atom (shown as dashed lines in Fig. 3.6). Note, however, that the value of s_0 at which the dimer prefactor is equal to the single atom prefactor depends strongly on the shape of the potential, in contrast to the barrier. Note also that the magnitude of the prefactor depends strongly on the shape parameter a; D_0 decreases with increasing a, in agreement with the single atom case. This result is intuitively reasonable: the prefactor can be thought of as an attempt frequency, and can be roughly identified with the vibration frequency of the atom or molecule at the bottom of the potential well [16]; a flatter well means a lower vibration frequency and therefore a lower prefactor.

Chapter 4

Diffusion Path Approximation

In this chapter we will develop an approximation method for multidimensional diffusion systems. The multidimensional problem will be reduced to a 1D problem by assuming that motion only occurs along the lowest energy path over the multidimensional potential energy surface, called the diffusion path approximation (DPA). This procedure will allow us to make use of analytical results available for 1D systems.

If there are multiple possible diffusion paths, the total hopping rate can be found by taking the sum of the different contributions, i.e.

$$\Gamma = \Gamma_1 + \Gamma_2 + \dots . \tag{4.1}$$

In the calculations in this thesis, however, we take the simpler approach of only considering the contribution from the lowest energy path.

In the next section we derive the formalism of the DPA, starting from the Langevin equations (2.16) derived in Chapter 2. In the following section we apply the DPA to a dimer moving in two dimensions (one parallel to the surface and one perpendicular).

4.1 Formalism

4.1.1 Langevin Equation in Reaction Coordinate

Consider a system of N adsorbed particles, which obeys the set of generalized Langevin equations derived in Chapter 2,

$$m_i \ddot{\vec{r}}_i + \int_0^t \sum_j \boldsymbol{B}_{ij} \cdot \dot{\vec{r}}_j(t')dt' + \nabla_{r_i} U_{\text{eff}}(\{\vec{r}_n\}) = \vec{\xi}_i(\{\vec{r}_n\}, t). \tag{4.2}$$

In the DPA, we assume that the particles only move on the lowest energy path between local minima. Let the curve followed by each particle on the diffusion path be given by $\sqrt{m_i}\vec{r}_i = \sqrt{m_0}\vec{f}_i(y)$, where m_0 is a mass scale which may be chosen

for convenience, and the curves are all parametrized by the total arc length y (the reaction coordinate), defined as

$$y = \int \left[\sum_i \left| \sqrt{\frac{m_i}{m_0}} d\vec{r}_i \right|^2 \right]^{1/2} = \int_{u_i}^{u_f} \left[\sum_i \left| \frac{d}{du} \vec{f}_i(u) \right|^2 \right]^{1/2} du, \tag{4.3}$$

where u is any parametrization of the curves. By standard rules of vector calculus, the curves then satisfy

$$\sum_i |\vec{f}_i'(y)|^2 = 1, \qquad \sum_i \vec{f}_i'(y) \cdot \vec{f}_i''(y) = 0, \tag{4.4}$$

where $\vec{f}_i' = \frac{d}{dy}\vec{f}_i$, and $\vec{f}_i'' = \frac{d^2}{dy^2}\vec{f}_i$.

Rewriting Eq. (4.2) in terms of the $\vec{f}_i$ gives

$$\begin{aligned} &\sqrt{m_i m_0}(\vec{f}_i''(y)\dot{y}^2 + \vec{f}_i'(s)\ddot{y}) + \int_0^t \sum_j \sqrt{\frac{m_0}{m_j}} \boldsymbol{B}_{ij} \cdot \vec{f}_j'[y(t')]\dot{y}(t')dt' \\ &+ \nabla_{r_i} U_{\text{eff}}(\{\vec{r}_n\}) = \vec{\xi}_i(\{\vec{r}_n\}, t). \end{aligned} \tag{4.5}$$

Taking the dot product of this equation with $\sqrt{m_0/m_i}\vec{f}_i'(y)$ and summing over i gives a generalised Langevin equation for y:

$$\begin{aligned} &m_0\ddot{y} + \int_0^t \sum_{i,j} \frac{m_0}{\sqrt{m_i m_j}} \vec{f}_i'[y(t)] \cdot \boldsymbol{B}_{ij} \cdot \vec{f}_j'[y(t')]\dot{y}(t')dt' \\ &+ \sum_i \sqrt{\frac{m_0}{m_i}} \nabla_{r_i} U_{\text{eff}}(\{\vec{r}_n\}) \cdot \vec{f}_i'(y) = \sum_i \sqrt{\frac{m_0}{m_i}} \vec{\xi}_i(\{\vec{r}_n\}, t) \cdot \vec{f}_i'(y). \end{aligned} \tag{4.6}$$

or

$$m_0\ddot{y} + \int_0^t B_y \dot{y}(t')dt' + \frac{d}{dy} U_{\text{eff}}(y) = \xi_y(y, t), \tag{4.7}$$

where B_y and ξ_y are given by

$$B_y = \sum_{i,j} \frac{m_0}{\sqrt{m_i m_j}} \vec{f}_i'[y(t)] \cdot \boldsymbol{B}_{ij} \cdot \vec{f}_j'[y(t')] \tag{4.8}$$

$$\xi_y(y, t) = \sum_i \sqrt{\frac{m_0}{m_i}} \vec{\xi}_i(\{\vec{r}_n\}, t) \cdot \vec{f}_i'(y). \tag{4.9}$$

Making use of the approximation for the memory-friction tensor derived in § 2.2, Eq. (2.73), gives

$$m_0\ddot{y} + \beta_y\dot{y} + \frac{d}{dy}U_{\text{eff}}(y) = \xi_y, \tag{4.10}$$

with

$$\begin{aligned}\beta_y &= \frac{3\pi}{2m_s\omega_D^3}\sum_{i,j}\frac{m_0}{\sqrt{m_i m_j}}\vec{f}_i'(y)\cdot\nabla_{r_i}\nabla_r V_{MS}^{(0)}(y)\cdot\nabla_{r_j}\nabla_r V_{MS}^{(0)}(y)\cdot\vec{f}_j'(y)\\ &= \frac{3\pi}{2m_s\omega_D^3}\left|\frac{d}{dy}\nabla_r V_{MS}^{(0)}(y)\right|^2.\end{aligned} \tag{4.11}$$

The random force has the following statistical properties

$$\begin{aligned}&\langle\xi_y(\{\vec{r}_n(t)\},t)\rangle = 0,\\ &\langle\xi_y(\{\vec{r}_n(t)\},t)\xi_y(\{\vec{r}_n(t')\},t')\rangle = 2k_BT\beta_y\delta(t-t').\end{aligned} \tag{4.12}$$

With Eq. (4.10) we now have a simple 1D Langevin equation that can be used to study the dynamics of an adsorbed molecule. The approximation that the molecule does not deviate from the lowest energy path will be most valid in the low temperature, high barrier regime, where the energy barrier ΔV is large compared to k_BT. It will also be most useful when there is a single dominant diffusion mechanism.

We can use Eq. (4.10) to calculate the diffusion coefficient with respect to the coordinate y,

$$D_y = \lim_{t\to\infty}\frac{\langle y^2\rangle}{2t}, \tag{4.13}$$

again using the high friction result given in Chapter 1,

$$D_y = k_BT\left[\frac{1}{l_y}\int_0^{l_y}\beta_y(y)\exp(U_{\text{eff}}(y)/k_BT)dy\frac{1}{l_y}\int_0^{l_y}\exp(-U_{\text{eff}}(y')/k_BT)dy'\right]^{-1}. \tag{4.14}$$

A more experimentally relevant quantity, however, is the center of mass diffusion coefficient

$$\boldsymbol{D} = \lim_{t\to\infty}\frac{\langle\vec{r}\vec{r}\rangle}{2t}. \tag{4.15}$$

To relate D_y to $\boldsymbol{D}$ suppose that moving along one period of the lowest energy path gives a displacement in the center of mass coordinate of magnitude l along the unit vector $\hat{a}$, and a displacement of l_y in the reaction coordinate y. Then we can write the coordinates $\vec{r}$ and y in the following form:

$$\vec{r} = n\hat{a}l + \hat{a}\delta r \qquad\qquad y = nl_y + \delta y, \tag{4.16}$$

where n is an integer, and $\delta r < l$, $\delta y < l_y$. In the long time limit, $t \to \infty$, n will be very large, so

$$\lim_{t\to\infty} \frac{\vec{r}}{y} = \frac{\hat{a}l}{l_y}. \tag{4.17}$$

We then have the following relationship between D_y and $\boldsymbol{D}$:

$$\boldsymbol{D} = \lim_{t\to\infty} \frac{\langle(\vec{r}\vec{r}/y^2)y^2\rangle}{2t} = \left(\frac{l}{l_y}\right)^2 \hat{a}\hat{a}D_y. \tag{4.18}$$

4.1.2 Minimum Energy Path

In order to make use of the DPA and calculate the integrals in Eq. (4.14), we must find the minimum energy path across the potential energy surface $U_{\text{eff}}(\{\vec{r}_n\})$ (the diffusion path). The first step is to find the transition state, i.e. the maximum along the minimum energy path, which is defined by the following properties. Consider a potential U that depends on the coordinates x_i, at a point on the surface $x_i = x_{0i}$ with $\nabla U = 0$. It can be expanded in a Taylor series,

$$U = U_0 + \frac{1}{2}\sum_{i,j} H_{ij}(x_i - x_{0i})(x_j - x_{0j}), \tag{4.19}$$

where $U_0 = U(\{x_0 i\})$, and H_{ij} are the elements of the Hessian matrix,

$$\boldsymbol{H} = \begin{pmatrix} \frac{\partial^2 U}{\partial x_1^2} & \frac{\partial^2 U}{\partial x_1 \partial x_2} & \cdots \\ \frac{\partial^2 U}{\partial x_2 \partial x_1} & \frac{\partial^2 U}{\partial x_2^2} & \cdots \\ \vdots & \vdots & \ddots \end{pmatrix}, \tag{4.20}$$

with all derivatives evaluated at $x_i = x_{0i}$. Changing to a set of coordinates η_i that diagonalizes $\boldsymbol{H}$, we have

$$U = U_0 + \frac{1}{2}\sum_i \lambda_i \eta_i^2, \tag{4.21}$$

where λ_i are the eigenvalues of $\boldsymbol{H}$. Coordinates with a positive eigenvalue correspond to a minimum of U, and those with a negative eigenvalue correspond to a maximum. A transition state can therefore be characterized as a point where the gradient is 0 and one eigenvalue of the Hessian matrix is negative, with the rest being positive. The diffusion path is found by following the steepest descent path from the transition state to the minimum; that is, following the direction of $-\nabla V$. To find the steepest descent path associated with a given transition state, a method developed by Page et al. [46] which employs a local quadratic approximation at each step was employed for the calculations that follow.

The location of transition states on a multidimensional potential surface is a complicated problem, and several methods have been developed [47]. We use an eigenvalue following method proposed by Cerjan and Miller [48], and developed further by Wales [49–51]. This method has the advantage that an accurate guess for the location of a transition state is not required as a starting point in order for the search to converge. We will give a brief outline of the method here.

At each point in the search for the transition state, the potential is approximated by its second order Taylor series, which, when written in the basis of the eigenvectors of the Hessian matrix, has the following form

$$U = U_0 + \sum_i g_i \eta_i + \frac{1}{2} \sum_i \lambda_i \eta_i^2, \tag{4.22}$$

where g_i is the first derivative of U along the ith eigenvector. The basic idea is to take a step along one eigenvector in a direction that increases the potential, and along all other eigenvectors in a direction that decreases the potential. The step sizes are determined by a Lagrange multiplier method (for details see Refs. [48, 49, 52]), resulting in the following expression

$$\Delta\eta_i = \pm \frac{2g_i}{|\lambda_i| + \sqrt{\lambda_i^2 + 4g_i^2}}, \tag{4.23}$$

where the + sign is used for energy maximization, and the − sign for minimization. Using this procedure, one of the eigenvectors can be followed in the "uphill" direction until a location with $\nabla U = 0$ is found. It can then be verified that it is a transition state (and not a minimum or higher order saddle point) by checking that one of the eigenvalues λ_i is negative and the rest are positive.

To systematically search the potential energy surface for transition states, we begin at a known local minimum, and use the algorithm outlined in Ref. [53]:

1. Begin at a known minimum on the potential energy surface, and take a small initial step in a random direction (necessary since the step size (4.23) is zero at a minimum).

2. Search along one of the eigenvectors until an extremum is found (or a set maximum number of steps is exceeded).

3. If the extremum is a transition state, take a small step along the direction with negative eigenvalue, and then follow the steepest descent path to the minimum to obtain the diffusion path.

4. Repeat the search following the other direction along the same eigenvector, and then both directions along all other eigenvectors.

5. Repeat the whole procedure with a new random initial step until a specified number of transition states have been found (or a set maximum number of searches have been conducted).

This method does not guarantee that all transition states are found, but previous studies indicate that it is very effective at finding all transition states in the vicinity of the starting point [49, 54, 55]. Since we start from the known lowest energy local minimum, and we only require the lowest energy diffusion path, any possible higher energy transition states or minima are irrelevant.

4.2 Dimer Diffusion in Two Dimensions

As a simple application of the Langevin equation derived in the previous section, we will now consider the diffusion of a dimer which moves along a 1D channel on a surface, and is also free to move in the direction perpendicular to the surface (thus accounting for both center of mass movement and rotation).

We will make use of the DPA to calculate the center of mass diffusion coefficient

$$D = \lim_{t\to\infty} \frac{\langle r_x^2 \rangle}{2t} \tag{4.24}$$

for the dimer in 2D (where r_x is the component of the dimer center of mass in the x direction along the surface). In the high barrier regime, $\Delta V \gg k_B T$, Eq. (4.14) for the diffusion coefficient gives rise to the Arrhenius form for D,

$$D = D_0 e^{-\Delta V/k_B T}, \tag{4.25}$$

as seen in Chapter 3. Since this is the regime most relevant to experiments, we will confine our calculations to high barriers. The prefactor D_0 and energy barrier ΔV are found by the same fitting procedure as in Chapter 3. For all calculations, the temperature range $40 < V_0/k_B T < 45$ was used.

4.2.1 Interaction Potential

The interaction potential can be expanded in a Fourier series in the coordinate along the surface, x,

$$V(x,z) = \sum_i v_i(z) \cos\left(\frac{2\pi i}{l} x\right). \tag{4.26}$$

We will keep only the first two terms in the series, and for both $v_0(z)$ and $v_1(z)$ we will use a Morse potential, allowing for differing strengths. The total potential is then

$$V(x,z) = V_0 \left(1 + A\cos\left(\frac{2\pi}{l}x\right)\right)\left(e^{-2a(z-z_0)} - 2e^{-a(z-z_0)}\right), \tag{4.27}$$

where A is a numerical constant which must satisfy $|A| < 1$ to prevent the potential from going to $-\infty$ when z becomes negative. We will also take $A > 0$, since allowing negative values for A simply shifts the potential in x by $l/2$, which does not change the diffusion behavior. Some plots of this potential for several values of A are given in Fig. 4.1. As can be seen from the figure, increasing A increases the corrugation along the surface. The minima are located at $x = (n + 1/2)l, z = z_0$, and the transition states are located at $x = nl, z = z_0$, where n is an integer. The energy barrier is $\Delta V = 2V_0 A$.

Considering now a dimer of two equal mass atoms with coordinates $\vec{r}_1 = (x_1, z_1)$ and $\vec{r}_2 = (x_2, z_2)$, we write the interaction potential in terms of the center of mass coordinate $\vec{r} = (\vec{r}_1 + \vec{r}_2)/2$ and the relative coordinate $\vec{s} = \vec{r}_1 - \vec{r}_2$,

$$V_{MS}(\vec{r}, \vec{s}) = v_x(r_x + s_x/2)v_z(r_z + s_z/2) + v_x(r_x - s_x/2)v_z(r_z - s_z/2), \tag{4.28}$$

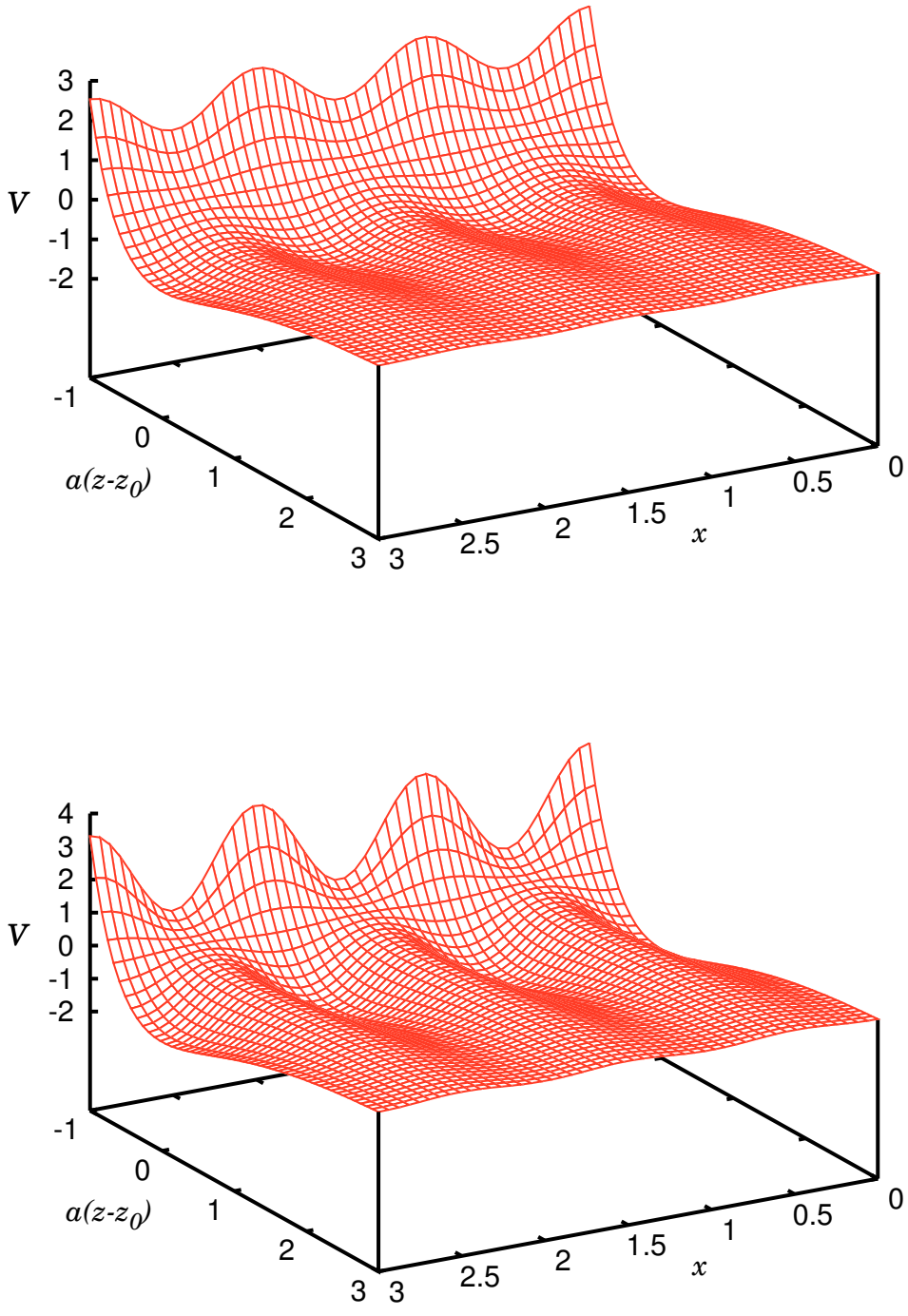

Figure 4.1: Adatom-surface interaction potential in 2D. The top figure is for $A = 0.3$, and the bottom is for $A = 0.7$.

where (r_x, r_z) and (s_x, s_z) are the x and z components of the center of mass and relative coordinates, and

$$v_x(x) = 1 + A\cos\left(\frac{2\pi}{l}x\right), \qquad v_z(z) = V_0\left(e^{-2a(z-z_0)} - 2e^{-a(z-z_0)}\right). \tag{4.29}$$

For the intramolecular potential we take a harmonic oscillator,

$$V_M(\vec{s}) = \frac{1}{2}k(|\vec{s}| - s_0)^2. \tag{4.30}$$

The total dimer potential is then

$$\begin{aligned} V(\vec{r},\vec{s}) &= V_{MS}(\vec{r},\vec{s}) + V_M(\vec{s}) \\ &= \frac{1}{2}k(|\vec{s}| - s_0)^2 + v_x(r_x + s_x/2)v_z(r_z + s_z/2) + v_x(r_x - s_x/2)v_z(r_z - s_z/2). \end{aligned} \tag{4.31}$$

In order to visualize the potential in Eq. (4.31), we show in figure 4.2 a plot of the potential as a function of r_x and the angle θ of $\vec{s}$ with respect to the x-axis, with r_z and $|\vec{s}|$ at the values that minimize the potential. Since the potential is periodic in r_x with period l and periodic in θ with period π, we take the ranges $0 < r_x < l/2$ and $0 < \theta < \pi$. It can be seen from the figures that there are two classes of local minima. One has $\theta = 0$ or $\theta = \pi$, corresponding to the dimer being flat against the surface. These minima have $r_z = z_0$ and either $r_x = nl$ or $r_x = (n + \frac{1}{2})l$. The other has $\theta = \pi/2$ or $\theta = 3\pi/2$, corresponding to the dimer standing vertically (i.e. perpendicular to the surface). These minima have $r_x = nl$.

Also shown in Fig. 4.2 are the lowest energy paths between the various local minima. The energy along these paths as a function of the reaction coordinate is shown in Fig. 4.3. Which path will be lowest in energy depends on the parameters of the potential. For example, increasing a makes the potential steeper in the z direction (the harmonic force constant at the bottom of the Morse potential is $2a^2V_0$), and so will increase the energy of the vertically stacked minimum. For the choice of parameters used in Figs. 4.2 and 4.3, the path along which the dimer stays flat against the surface is the lowest energy path.

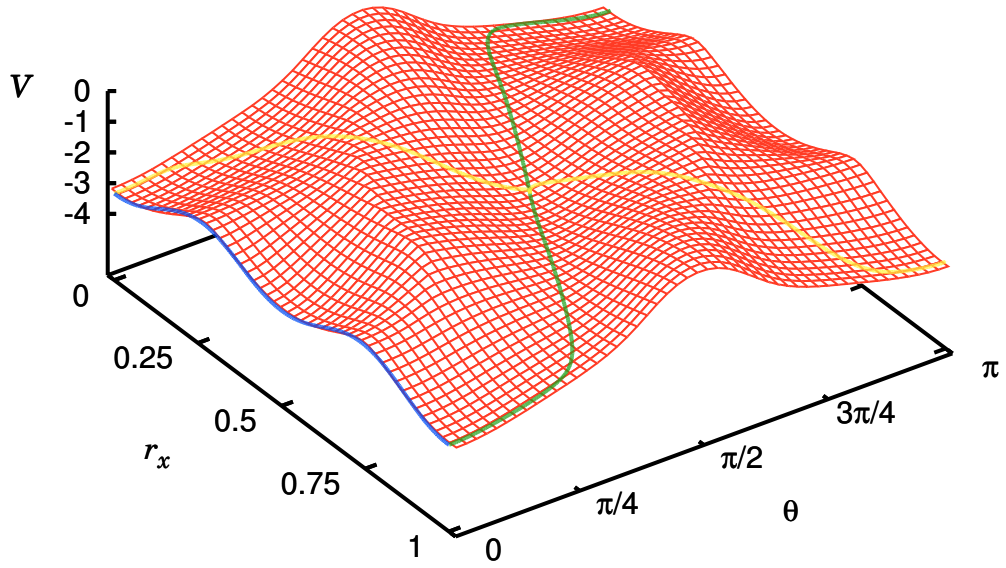

Figure 4.2: Potential energy minimized with respect to s_z and $|\vec{s}|$, with parameters $A = 0.7$, $a = 1.7/l$, $k = 3.5V_0/l^2$, $s_0 = 1.4l$.

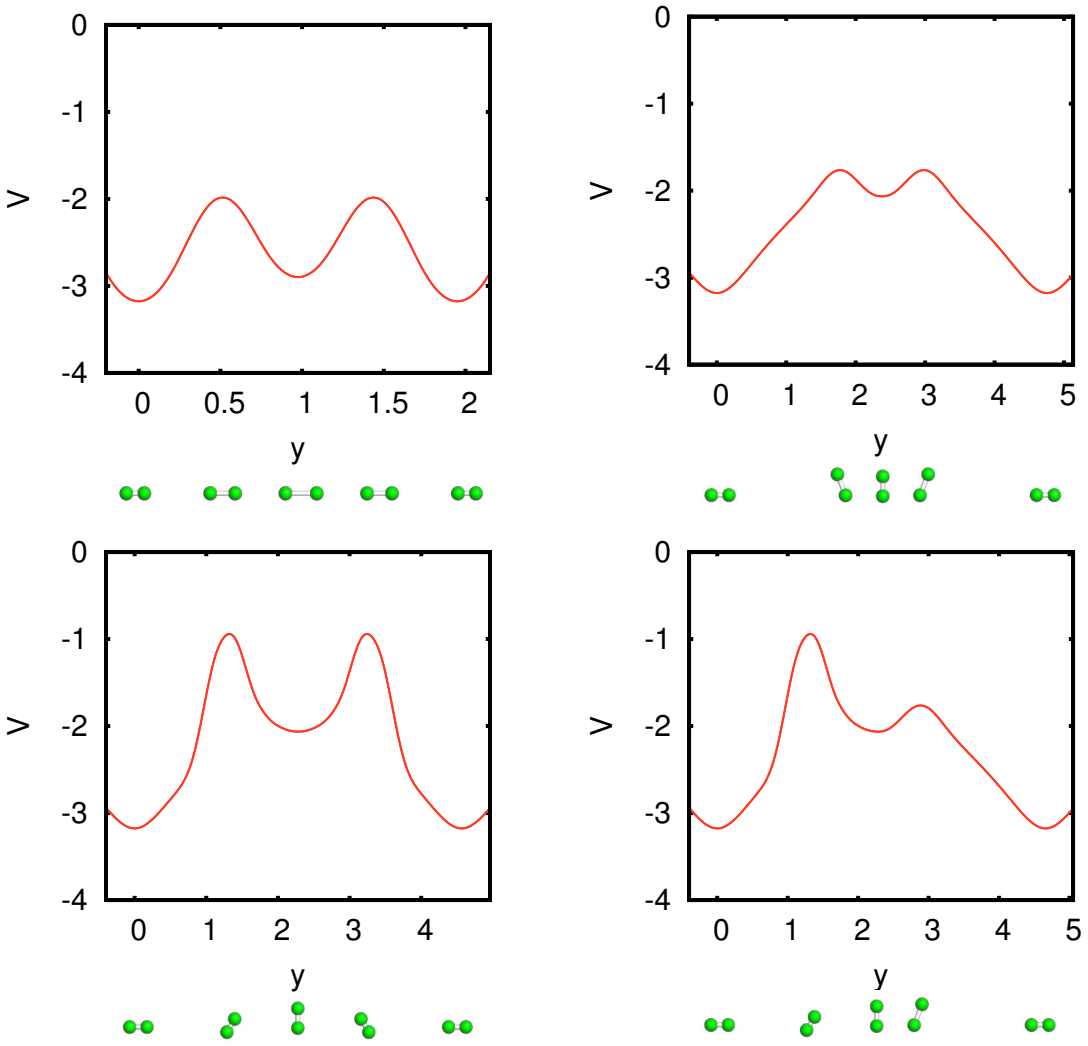

Figure 4.3: Energy along the lowest energy diffusion path for the potential energy surface (4.31) with parameters $A = 0.7$, $a = 1.7/l$, $k = 3.5V_0/l^2$, $s_0 = 1.4l$. The images beneath the graphs show the orientation of the dimer at the local minima and transition states.

4.2.2 Dimer Diffusion in One Dimension

Let us first consider a simpler case where the DPA can be compared to an exact solution of the Langevin equations (4.2). The special case we consider is an infinitely stiff dimer confined to 1D (the same system treated in Chapter 3), where the dimer-substrate interaction potential (4.28) becomes

$$V_{MS}(x_1, x_2) = -2V_0 - V_0 A \cos\left(\frac{2\pi}{l} x_1\right) - V_0 A \cos\left(\frac{2\pi}{l} x_2\right). \tag{4.32}$$

The Langevin equations for a dimer in 1D read

$$\begin{aligned} m\ddot{x}_1 + \beta_{11}\dot{x}_1 + \beta_{12}\dot{x}_2 + \frac{\partial}{\partial x_1}[V_{MS}(x_1, x_2) + V_M(x_1 - x_2)] &= \xi_1 \\ m\ddot{x}_2 + \beta_{21}\dot{x}_1 + \beta_{22}\dot{x}_2 + \frac{\partial}{\partial x_2}[V_{MS}(x_1, x_2) + V_M(x_1 - x_2)] &= \xi_2. \end{aligned} \tag{4.33}$$

Adding the two equations gives, in terms of the center of mass and relative coordinates,

$$M\ddot{r} + (\beta_{11} + \beta_{21})\dot{x}_1 + (\beta_{12} + \beta_{22})\dot{x}_2 + \frac{\partial}{\partial r} V_{MS}(r, s) = \xi_r, \tag{4.34}$$

where $\xi_r = \xi_1 + \xi_2$, and $M = 2m$ is the total mass of the dimer. If the dimer is infinitely stiff, then the two atoms are at a fixed separation, $x_1 = x_2 + s_0$, and $\dot{x}_1 = \dot{x}_2 = \dot{r}$. The above equation then becomes

$$M\ddot{r} + \beta_r \dot{r} + \frac{\partial}{\partial r} V_{MS}(r, s_0) = \xi_r, \tag{4.35}$$

where, making use of Eq. (2.73),

$$\begin{aligned} \beta_r &= \beta_{11} + \beta_{21} + \beta_{21} + \beta_{22} \\ &= \frac{3\pi}{2m_s\omega_D^3}\left[\left(\frac{\partial^2 V_{MS}}{\partial x_1 \partial r}\right)^2 + \left(\frac{\partial^2 V_{MS}}{\partial x_2 \partial r}\right)^2 + 2\frac{\partial^2 V_{MS}}{\partial x_1 \partial r}\frac{\partial^2 V_{MS}}{\partial x_2 \partial r}\right]. \end{aligned} \tag{4.36}$$

Using the fact that V_{MS} has the form $V_{MS}(x_1, x_2) = v(x_1) + v(x_2)$, i.e. pairwise interactions, the friction coefficient for the stiff dimer can be written as

$$\beta_r = \frac{3\pi}{2m_s\omega_D^3}\left(\frac{\partial^2 V_{MS}}{\partial r^2}\right)^2, \tag{4.37}$$

which is the same expression used in the stiff dimer calculations in Chapter 3, Eq. (3.14). Eq. (4.35) is therefore equivalent to the center of mass Langevin equation

derived in Chapter 2 for a more general case. The diffusion coefficient is given by Eq. (3.15), which in the present notation reads

$$D = \bar{D}\frac{1}{48A\pi^5\cos(\frac{\pi}{l}s_0)I_0(\gamma)[bI_0(\gamma) - I_1(\gamma)]}, \tag{4.38}$$

where $\gamma = 2AV_0\cos(\frac{\pi}{l}s_0)/k_BT$. In the limit of high barriers, this becomes

$$D = \bar{D}\frac{1}{24A\pi^4|\cos(\frac{\pi}{l}s_0)|}e^{-4AV_0|\cos(\frac{\pi}{l}s_0)|/k_BT}. \tag{4.39}$$

In Fig. 4.4 we compare the diffusion prefactor and barrier for the stiff dimer, given by Eq. (4.39), and the corresponding results for a flexible dimer in the DPA. It can be seen that the DPA results become closer to the stiff dimer result as the dimer stiffness k is increased. In fact it is easy to see that the stiff dimer approximation and the DPA become equivalent in the limit $k \to \infty$. In this case, the reaction coordinate y is simply the center of mass of the dimer r, in which case the DPA friction coefficient, Eq. (4.11), and that of the stiff dimer, Eq. (4.37), become equal, $\beta_y = \beta_r$. The two Langevin equations are then identical, and so the diffusion coefficients are also identical.

Also shown in Fig. 4.4 is the stiff dimer result of Ruckenstein and Tsekov [9],

$$D = \bar{D}\frac{|\cos(\frac{\pi}{l}s_0)|}{12A\pi^4}e^{-4AV_0|cos(\frac{\pi}{l}s_0)|/k_BT}. \tag{4.40}$$

To obtain their result, Ruckenstein and Tsekov start with the following set of Langevin equations for the atoms of the dimer

$$\begin{aligned} m\ddot{x}_1 + \beta_0\dot{x}_1 + \frac{\partial}{\partial x_1}(V_{MS} + V_M) &= \xi_1 \\ m\ddot{x}_2 + \beta_0\dot{x}_2 + \frac{\partial}{\partial x_2}(V_{MS} + V_M) &= \xi_2, \end{aligned} \tag{4.41}$$

where β_0 is a constant friction coefficient $\beta_0 = \frac{3\pi}{2m_s\omega_D^3}A^2V_0^2(\frac{2\pi}{l})^4$, resulting in the following center of mass equation

$$M\ddot{r} + 2\beta_0\dot{r} + \frac{\partial}{\partial r}V_{MS}(r, s_0) = \xi_r. \tag{4.42}$$

The constant friction coefficient β_0 is that of a single atom in the cosine potential $AV_0\cos(\frac{2\pi}{l}x)$, evaluated at the transition state [9], as discussed in § 3.2.

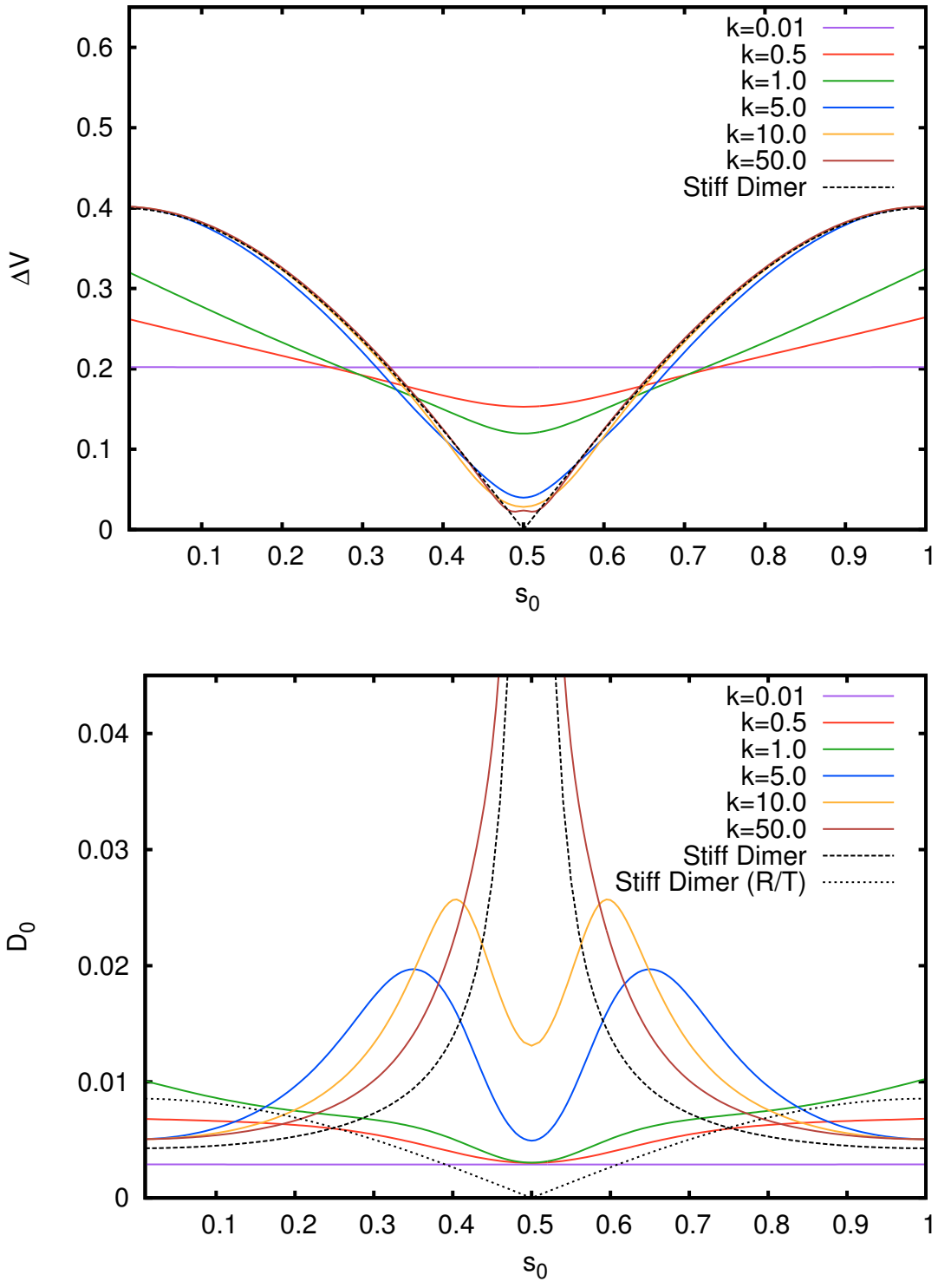

Figure 4.4: Diffusion coefficient prefactor and barrier as a function of s_0 for various values of the dimer stiffness k (in the legend, k is listed in units of V_0/l^2). The other parameters in the potential are $A = 0.1$ and $a = 2.0/l$.

The energy barrier in Eq. (4.40) is the same as our result, Eq. (4.39), but the prefactor is qualitatively different, as seen in Fig. 4.4. Interestingly, although Eq. (4.40) is obtained in the stiff dimer limit, it has the same qualitative shape as the DPA results for a weakly bonded dimer. To understand this unexpected result, consider the DPA in the limit $k \to 0$. In this limit the minimum energy configuration will have each atom of the dimer at a minimum of the cosine potential, $x_1, x_2 = nl$ (where n is an integer), and the diffusion will proceed by one atom hopping to a neighboring minimum while the second remains fixed. The transition state will then occur when one atom is at a minimum and the other is at a maximum, $x_1 = (n_1 + \frac{1}{2})l$, $x_2 = n_2 l$, and it can easily be shown that the DPA friction coefficient at the transition state is $\beta_y = \beta_0$. In the DPA the potential will be given by Eq. (4.32) with one atom fixed at a minimum, i.e. $V(y) = -2V_0 - AV_0 - AV_0 \cos(\frac{2\pi}{l}y)$. Compare these with the friction coefficient and potential energy used in Eq. (4.42), $2\beta_0$ and $V(r) = 2V_0 - 2AV_0 \cos(\frac{\pi}{l}s_0)\cos(\frac{2\pi}{l}r)$, respectively. For the $k \to 0$ limit of the DPA, both the friction coefficient and the potential along the diffusion path are independent of the dimer length. In Ruckenstein and Tsekov's calculation, the friction coefficient is also independent of s_0, and differs only by a factor of 2. The potential energy, however, does depend on s_0, and only coincides with the DPA potential at $s_0 = l/3$ (ignoring the constant term). It can be verified in Fig. 4.4 that the energy barriers ΔV for the stiff dimer result and the $k \to 0$ DPA result do indeed agree at $s_0 = l/3$.

4.2.3 Dimer Diffusion in Two Dimensions

We now consider the diffusion of a dimer in the two dimensional potential Eq. (4.31) that moves across the surface by rotating, as shown in Figs. 4.2 and 4.3. Such diffusion paths in the potential (4.31) will always contain both a vertically stacked configuration and a flat configuration, either of which can be a local minimum or a transition state. The effects of each of the parameters in the potential on the diffusion coefficient are considered in turn.

We first consider the dependence of the diffusion coefficient on the equilibrium dimer length s_0. When the dimer length is short (compared to $1/a$), rotating the dimer out of the horizontal plane will not raise the energy significantly, and there is

the possibility of a local minimum with the dimer standing vertically. For a situation where this vertically stacked minimum is lowest in energy, the diffusion will then proceed by a rotational motion. If the dimer length s_0 is then increased, the atom on top will be forced further away from the surface, and if the desorption energy is large compared to the diffusion barrier (as is typically the case), this will cause the vertically stacked minima to become higher in energy than the flat minima. Once s_0 is large enough that the flat diffusion path is lowest in energy, a further increase in s_0 should give a periodic dependence of the barrier and prefactor, similar to Fig. 4.4. This behavior can be seen in Fig. 4.5, where the energy barrier and prefactor are plotted as a function of s_0. At $s_0 = 0.86l$, the diffusion path for which the dimer stays flat against the surface becomes lowest in energy. This is particularly noticeable in the graph of the prefactor, where there is a discontinuous jump between the prefactors for the rotating and flat diffusion paths at $s_0 = 0.86l$. Note that we have calculated the diffusion coefficient considering only the lowest energy path, in order to emphasize the change in lowest energy path from rotating to flat. However, if contributions from both paths had been considered, in the manner of Eq. (4.1), the discontinuous jump in Fig. 4.5 would be smoothed out.

Next we consider the dependence of the diffusion coefficient on the parameter a, which determines the steepness of the potential in the direction perpendicular to the surface (z direction). Plots of the prefactor and barrier vs a are shown in Fig. 4.6. The parameters are chosen so that for small a the vertically stacked minimum has the lowest energy. Increasing a makes the potential more steep in the z direction, and therefore makes the vertically stacked minima less favorable. As a is increased, eventually the flat minima become lower in energy, and the diffusion path for which the dimer stays always flat against the surface (with $z_1 = z_2 = z_0$) is the lowest energy diffusion path. Increasing a further after this point has no effect on the prefactor or barrier, since the 1D potential, Eq. (4.32) is independent of a.

Previous studies have found [56], however, that the vibration frequency of an ad-particle in the direction perpendicular to the surface can in some cases have a significant effect on the magnitude of the diffusion coefficient. That this effect is absent in the present calculations is a reflection of the fact that all motion perpendicular to

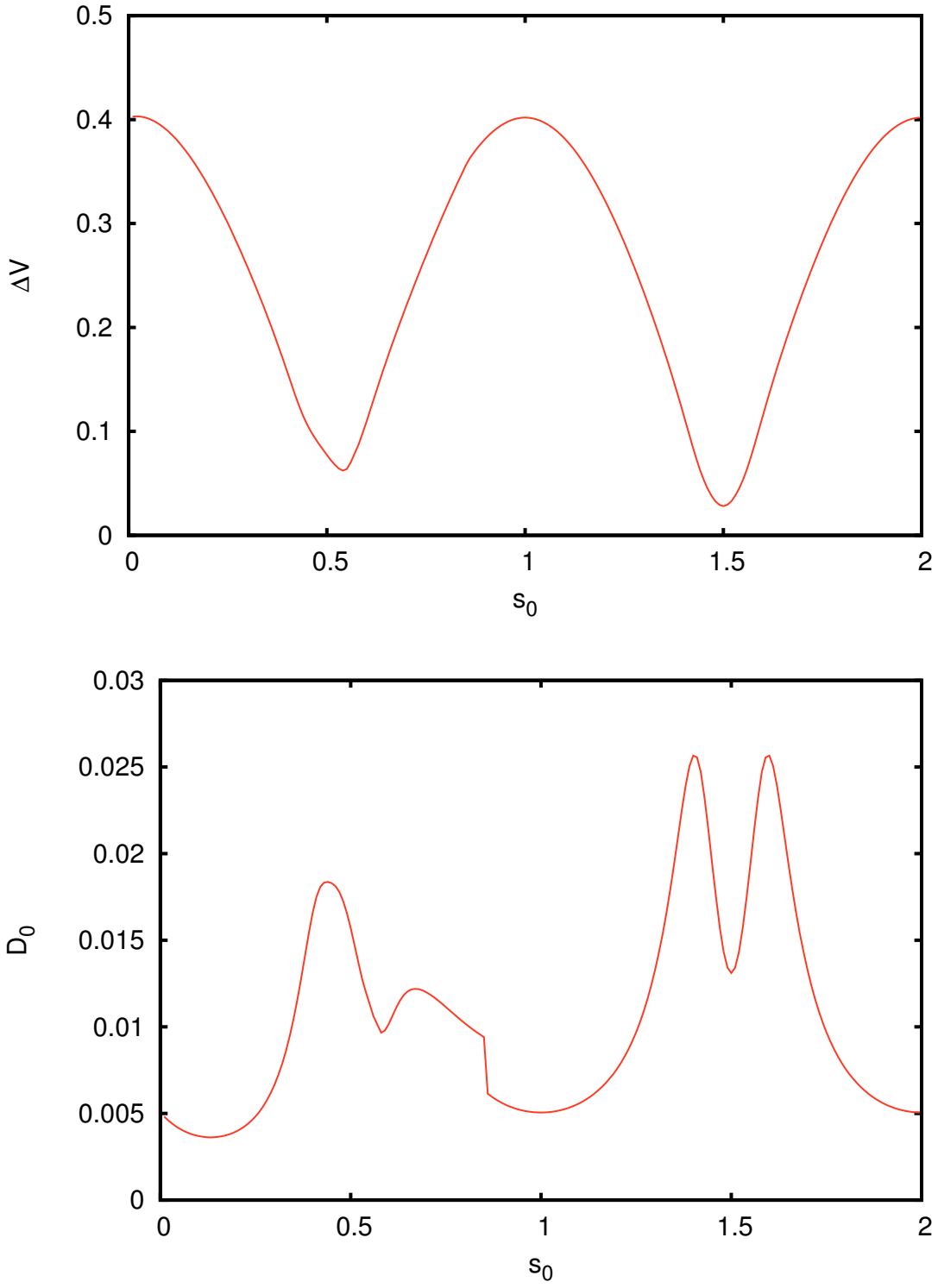

Figure 4.5: Diffusion coefficient prefactor and barrier as a function of s_0. The other parameters in the potential are $A = 0.1$, $a = 1.0/l$, and $k = 10.0V_0/l^2$.

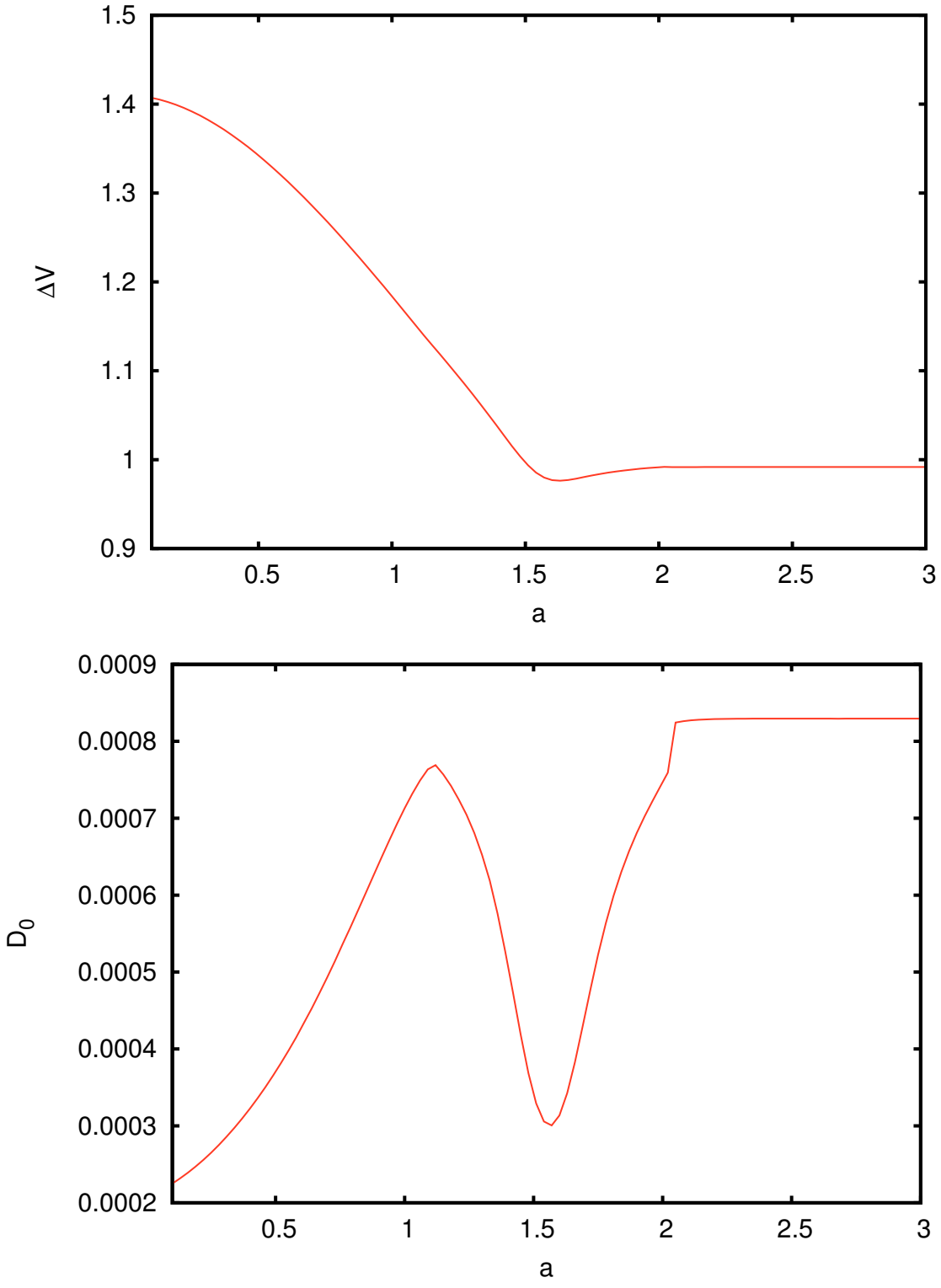

Figure 4.6: Diffusion coefficient prefactor and barrier as a function of a. The other parameters in the potential are $A = 0.7$, $k = 10.0V_0/l^2$, and $s_0 = 0.6l$.

the lowest energy diffusion path is ignored.

Finally, we consider the dependence of the diffusion coefficient on the dimer stiffness k. Plots of the prefactor and barrier vs k are shown in Fig. 4.7. In Fig. 4.7 the parameters have been chosen so that the lowest energy minimum is a vertically stacked configuration at $r_x = 0$. The flat configuration at $r_x = l/2$ is either the transition state or a local minimum. Increasing the dimer stiffness k will force the dimer to be closer to its equilibrium length s_0. Since we have chosen an equilibrium length incommensurate with the lattice constant, $s_0 = 0.4l$, this will move the atoms of the dimer away from the adsorption sites, raising the energy of the flat configuration. It will also raise the energy of the vertically stacked configuration, since when vertically stacked, the dimer is compressed to shorter than s_0, so increasing k will move the top atom further away from the surface. It is therefore not immediately obvious what effect increasing k should have on the difference between the energy of the two configurations, i.e. the energy barrier ΔV. It can be seen from Fig. 4.7 that increasing k in fact increases the energy barrier, implying that the effect on the energy of the vertically stacked configuration is less significant than the effect on the flat configuration. The prefactor can be seen to increase sharply in the range $0 \lesssim k \lesssim 15$, after which it levels out, approaching the stiff dimer limit.

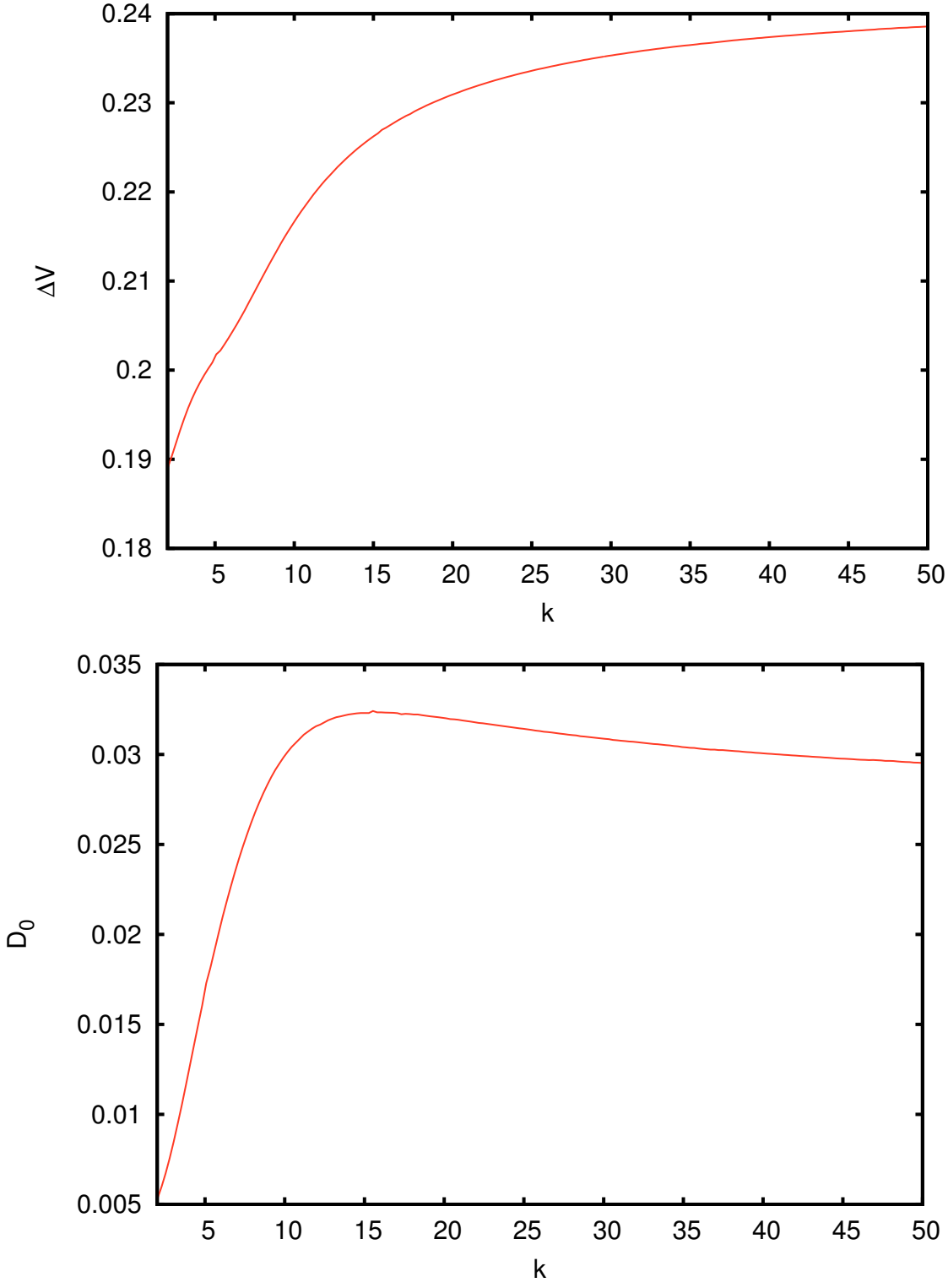

Figure 4.7: Diffusion coefficient prefactor and barrier as a function of k (shown in units of V_0/l^2). The other parameters in the potential are $A = 0.1$, $a = 0.5/l$, and $s_0 = 0.4l$.

Chapter 5

Conclusions

In this thesis, we have derived a generalized Langevin equation for surface diffusion starting from a microscopic classical mechanical model. We then employed the Markov approximation to obtain a standard Langevin equation, appropriate for systems with a separation in time scales between the vibrational and translation motion of the adsorbed molecule.

We first applied this equation to study a stiff dimer diffusing along a 1D channel on a surface, calculating the diffusion coefficient for the center of mass motion. An interesting dependence of the diffusion prefactor on the equilibrium length of the dimer was found (shown in Fig. 3.6), and explained in terms of the appearance of local minima in the dimer potential. A strong dependence of the prefactor on the shape of the potential was also found. The energy barrier was seen to depend periodically on the dimer length, being a maximum when the dimer was commensurate with the lattice ($s_0 = nl$) and a minimum when the dimer was incommensurate with the lattice ($s_0 = (n + 1/2)l$), as seen in previous work [9].

We also showed that our newly derived expression for the friction coefficient of a stiff dimer in 1D, which takes full account of the dependence of the friction on the dimer length and position, produced significantly different results for the prefactor compared to previous calculations. This suggests that our new approach to the surface diffusion of molecules, derived in Chapter 2, provides a significant modification to previous studies based on Langevin equations.

Next we developed an approximation method to reduce a multi-dimensional vibrating system to 1D (the DPA), applicable to an arbitrarily complex adsorbed molecule. We applied this approximation to diffusion of a flexible dimer diffusing in 1D along a surface, and also free to rotate perpendicular to the surface. For diffusion paths where the dimer remains flat against the surface, the results of Chapter

3 for the infinitely stiff dimer were recovered in the limit of large dimer stiffness. Comparison of the DPA results to the stiff dimer results from Chapter 3 also helped to explain and clarify the differences between our results for the stiff dimer in 1D and those of previous studies [9].

In the future it would be interesting to apply this approach to a large organic molecule adsorbed on a metal surface. Interesting diffusion behavior has been observed recently in many such systems. For example, for porphyrin molecules adsorbed on a copper surface the diffusion is strictly one dimensional along the molecular main axis, a result of a conformational adaptation upon adsorption. In the same system, when two porphyrin molecules come together they can form dimers, and the hopping rate for the dimers is larger than that for the monomers by two orders of magnitude [36]. Other systems show novel behavior, such as supramolecular self-assembly [39], and a "lock-and-key" effect, where a diffusing molecule is immobilized by rotating it with respect to the surface using an STM tip [33]. Such systems present a challenge for molecular dynamics methods due to the large number of atoms involved. The method outlined in this thesis provides the means to simplify the theoretical description by averaging over the internal vibrations of a large molecule, while still retaining information about the microscopic interactions by way of the expression for the friction tensor derived in Chapter 2.

For a full description of the coupling of an adsorbed molecule to the surface, the electronic degrees of freedom must be taken into account. So far electronic interactions have not been incorporated into a Langevin or Fokker-Planck type description of surface diffusion, and doing so represents a possible direction for future research. To include the electronic degrees of freedom requires one to start with a microscopic model based on quantum mechanics. Such a model has been worked out [7], and could serve as the starting point for a Fokker-Planck equation for surface diffusion that takes full account of the electronic interactions. Another interesting possibility is to compare the quantum Fokker-Planck equation derived in Ref. [7] to the classical version obtained from the Langevin equation derived in this thesis, and in Ref. [13]. Such a comparison has already been made between quantum and classical versions of the Fokker-Planck equation for desorption, where it was found that the quantum

version reduces to the low friction limit of the classical version upon ignoring terms of the order of the thermal fluctuations [57].

Bibliography

[1] Pimpinelli, A. and Villain, J. February 1998 Physics of crystal growth, volume **35**, Cambridge University Press, .

[2] Jensen, P. (1999) *Reviews of Modern Physics* **71(5)**, 1695–1735.

[3] Ehrlich, G. and Hudda, F. G. (1966) *The Journal of Chemical Physics* **44(3)**, 1039–1049.

[4] Shiang, K. D. and Tsong, T. T. (1994) *Physical Review B* **49(11)**, 7670–7678.

[5] Barth, J. October 2000 *Surface Science Reports* **40(3-5)**, 75–149.

[6] Montalenti, F. and Ferrando, R. (1999) *Physical Review B* **59(8)**, 5881–5891.

[7] Azzouz, M., Kreuzer, H. J., and Shegelski, M. R. A. (2002) *Physical Review B* **66(12)**, 125403.

[8] Heinsalu, E., Patriarca, M., and Marchesoni, F. (2008) *Physical Review E* **77(2)**, 021129.

[9] Ruckenstein, E. and Tsekov, R. May 1994 *The Journal of Chemical Physics* **100(10)**, 7696–7699.

[10] Pijper, E. and Fasolino, A. (2005) *Physical Review B* **72(16)**, 165328.

[11] Fu, C.-C., Weissmann, M., and Saul, A. June 2001 *Surface Science* **481(1-3)**, 97–104.

[12] Montalenti, F., Baletto, F., and Ferrando, R. (2000) *Surface Science* **454-456**, 575–578.

[13] Tsekov, R. and Ruckenstein, E. (1994) *The Journal of Chemical Physics* **100(2)**, 1450–1455.

[14] Hänggi, P., Talkner, P., and Borkovec, M. (1990) *Reviews of Modern Physics* **62(2)**, 251–341.

[15] Braun, O. M. (2000) *Physical Review E* **63(1)**, 011102.

[16] Ala-Nissila, T., Ferrando, R., and Ying, S. C. (2002) *Advances in Physics* **51(3)**, 949–1078.

[17] Chen, L. Y., Baldan, M. R., and Ying, S. C. (1996) *Physical Review B* **54(12)**, 8856–8861.

[18] Ferrando, R., Spadacini, R., and Tommei, G. E. October 1993 *Physical Review E* **48(4)**, 2437–2451.

[19] Persson, B. N. J. (1991) *Physical Review B* **44(7)**, 3277–3296.

[20] vanKampen, N. G. (2007) Stochastic Processes in Physics and Chemistry, North Holland, 3 edition.

[21] Risken, H. (1989) The Fokker-Planck Equation, Springer-Verlag, .

[22] Fusco, C. and Fasolino, A. March 2003 *Thin Solid Films* **428(1-2)**, 34–39.

[23] Caratti, G., Ferrando, R., Spadacini, R., and Tommei, G. E. (1996) *Physical Review E* **54(5)**, 4708–4721.

[24] Kramers, H. A. (1940) *Physica* **7(4)**, 284–304.

[25] Banavar, J., Cohen, M., and Gomer, R. May 1981 *Surface Science* **107(1)**, 113–126.

[26] Mel'nikov, V. I. and Meshkov, S. V. (1986) *The Journal of Chemical Physics* **85(2)**, 1018–1027.

[27] FESTA, R. and DAGLIANO, E. February 1978 *Physica A: Statistical and Theoretical Physics* **90(2)**, 229–244.

[28] Chen, L. Y. and Ying, S. C. (1994) *Physical Review Letters* **73(5)**, 700–703.

[29] Kreuzer, H. J. and Gortel, Z. W. (1986) Physiosorption Kinetics, Springer Verlag, .

[30] Papousek, D. and Aliev, M. (1982) Molecular Vibrational-Rotational Spectra, Elsevier Scientific Publishing Company, .

[31] Wilson, E. B., Decius, J. C., and Cross, P. C. (1955) Molecular Vibrations, McGraw-Hill Book Company, New York.

[32] Miwa, J. A., Weigelt, S., Gersen, H., Besenbacher, F., Rosei, F., and Linderoth, T. R. March 2006 *Journal of the American Chemical Society* **128(10)**, 3164–3165.

[33] Otero, R., Hummelink, F., Sato, F., Legoas, S. B., Thostrup, P., Laegsgaard, E., Stensgaard, I., Galvao, D. S., and Besenbacher, F. October 2004 *Nature Materials* **3(11)**, 779–782.

[34] Gimzewski, J. K., Joachim, C., Schlittler, R. R., Langlais, V., Tang, H., and Johannsen, I. July 1998 *Science* **281(5376)**, 531–533.

[35] Stolt, K., Graham, W. R., and Ehrlich, G. (1976) *The Journal of Chemical Physics* **65(8)**, 3206–3222.

[36] Eichberger, M., Marschall, M., Reichert, J., Weber-Bargioni, A., Auwarter, W., Wang, R., Kreuzer, H., Pennec, Y., Schiffrin, A., and Barth, J. December 2008 *Nano Letters* **8(12)**, 4608–4613.

[37] Jung, T. A., Schlittler, R. R., and Gimzewski, J. K. April 1997 *Nature* **386(6626)**, 696–698.

[38] Weber-Bargioni, A., Auwärter, W., Klappenberger, F., Reichert, J., Lefrançois, S., Strunskus, T., Wöll, C., Schiffrin, A., Pennec, Y., and Barth, J. V. (2008) *ChemPhysChem* **9(1)**, 89–94.

[39] Auwärter, W., Klappenberger, F., Weber-Bargioni, A., Schiffrin, A., Strunskus, T., Wöll, C., Pennec, Y., Riemann, A., and Barth, J. V. September 2007 *Journal of the American Chemical Society* **129(36)**, 11279–11285.

[40] Tsekov, R. and Ruckenstein, E. December 1995 *Surface Science* **344(1-2)**, 175–181.

[41] Tsekov, R. and Smirniotis, P. G. November 1998 *The Journal of Physical Chemistry B* **102(47)**, 9385–9391.

[42] Persson, B. N. J. and Ryberg, R. (1985) *Physical Review B* **32(6)**, 3586–3596.

[43] Gradshteyn, I. S. and Ryzhik, I. M. January 1994 Table of Integrals, Series, and Products, Fifth Edition, Academic Press, 5th edition.

[44] Romero, A. H., Lacasta, A. M., and Sancho, J. M. (2004) *Physical Review E* **69(5)**, 051105.

[45] Braun, O. M., Ferrando, R., and Tommei, G. E. (2003) *Physical Review E* **68(5)**, 051101.

[46] Page, M. and James W. McIver, J. (1988) *The Journal of Chemical Physics* **88(2)**, 922–935.

[47] Olsen, R. A., Kroes, G. J., Henkelman, G., Arnaldsson, A., and Jónsson, H. (2004) *The Journal of Chemical Physics* **121(20)**, 9776–9792.

[48] Cerjan, C. J. and Miller, W. H. (1981) *The Journal of Chemical Physics* **75(6)**, 2800–2806.

[49] Wales, D. J. (1994) *The Journal of Chemical Physics* **101(5)**, 3750–3762.

[50] Wales, D. J. (1990) *Faraday Trans.* **86(21)**, 3505–3517.

[51] Wales, D. J. (1991) *Molecular Physics: An International Journal at the Interface Between Chemistry and Physics* **74(1)**, 1–25.

[52] Baker, J. (1986) *Journal of Computational Chemistry* **7(4)**, 385–395.

[53] Miller, M. A., Doye, J. P. K., and Wales, D. J. (1999) *The Journal of Chemical Physics* **110(1)**, 328–334.

[54] Wales, D. J. (1992) *Faraday Trans.* **88(5)**, 653–657.

[55] Wales, D. J., Miller, M. A., and Walsh, T. R. August 1998 *Nature* **394(6695)**, 758–760.

[56] Ala-Nissila, T. and Ying, S. C. (1990) *Physical Review B* **42(16)**, 10264–10274.

[57] Jack, D. B. and Kreuzer, H. J. (1982) *Physical Review B* **26(12)**, 6516–6529.